Battery Energy

WILEY

REVIEW OPEN ACCESS

Nitrogen-Doped Graphene Aerogels for Supercapacitors: Advances in Synthesis and Electrochemical Performance

Khaled Abdou Ahmed Abdou Elsehsah[1] | Zulkarnain Ahmad Noorden[1] | Norhafezaidi Mat Saman[1] | Noor Azlinda Ahmad[1] | Mohd Faizal Hasan[2] | Sharin Ab Ghani[3] | Ayaz Ahmed[1]

[1]Institute of High Voltage and High Current, Faculty of Electrical Engineering, Universiti Teknologi Malaysia, Johor Bahru, Johor, Malaysia | [2]Faculty of Mechanical Engineering, Universiti Teknologi Malaysia, Johor Bahru, Johor, Malaysia | [3]Faculty of Electrical Technology and Engineering, Universiti Teknikal Malaysia Melaka, Durian Tunggal, Melaka, Malaysia

Correspondence: Khaled Abdou Ahmed Abdou Elsehsah (ahmed-a2@graduate.utm.my) | Zulkarnain Ahmad Noorden (zulkarnain-an@utm.my)

Received: 5 August 2025 | **Revised:** 18 December 2025 | **Accepted:** 30 December 2025

Funding: Universiti Teknologi Malaysia, Grant/Award Numbers: Q.J130000.5009.10G17, Q.J130000.5023.10G18

Keywords: energy density | graphene aerogel | nitrogen-doped | specific capacitance | supercapacitor

ABSTRACT

Nitrogen-doped graphene aerogels (NGAs) have attracted much attention as next-generation electrode materials for supercapacitors because of their high surface area, excellent conductivity, and chemical tunability. Recent studies have confirmed how nitrogen doping can improve pseudocapacitive behaviour, wettability, and electron transport, thus significantly improving the specific capacitance, energy density, and cycling performance. This review analyses the different synthesis strategies, such as hydrothermal self-assembly, sol-gel polymerisation, and template-directed synthesis, and shows the electrochemical performance obtained from both symmetric and asymmetric set-ups. The best-performing NGAs have demonstrated specific capacitances reaching 900 F/g, energy densities of over 60 Wh/kg, and long-term retention exceeding 90% over 10,000 cycles. Nonetheless, multiple synthesis strategies are still limited by batch processing, excessive thermal demand, and difficulty with dopant homogeneity. Details on the electrode configuration and performance reported between studies are inconsistent, making direct comparisons challenging and hindering industrial translation. This review highlights the critical demand for scalable, greener synthesis protocols, standardised testing protocols, and systematic evaluations of the role of nitrogen species in capacitance enhancement. This work can be extended to dual-doping, flexible electrode fabrication, and the incorporation of the doped material into practical device architectures. Such insights provide a basis for rationally designing high-performance N-GAs for supercapacitors.

1 | Introduction

The need for energy storage devices has increased due to the rapid rise of portable gadgets, electric cars, and renewable energy systems. These systems require high-power energy storage technologies with extended cycle life and quick charge/discharge capabilities [1, 2]. Although lithium-ion batteries (LIBs) remain unmatched in their energy density, the high energy density brings corresponding drawbacks, such as safety concerns, low kinetics, and short cycle life under high-power expectations [3, 4]. Due to their widely improved power density, high charge-discharge rates, and excellent cycle stability, supercapacitors are considered an attractive complementary alternative [5]. They bridge the gap between conventional capacitors and batteries by combining fast energy supply and long cycling life, rendering them appropriate for high-performance applications [6]. Among the different types, the electric double-layer capacitors (EDLCs) store charge electrostatically at the electrode-electrolyte interface, and thus, the

surface area, porosity, and conductivity of the electrode material strongly prescribe their performance [7, 8].

Because of their excellent stability and conductivity, carbon-based materials such as activated carbon, carbon nanotubes, and carbon nanofibers are being researched extensively as EDLC electrodes. Although there are many different types of carbonaceous materials, graphene, a two-dimensional monolayer of sp^2-bonded carbon atoms, has been appealing for various supercapacitor (SC) applications due to its remarkable electrical conductivity, high specific surface area (~2600 m^2/g), mechanical strength, and electrochemical stability [6, 9, 10]. These characteristics identify graphene as an electrode material with significant potential for SC applications.

However, in practical applications, the restacked or agglomerated graphene sheets reduce the effective surface area due to the limited accessibility of ions. These challenges were addressed with the development of 3D graphene aerogels (GAs). The aerogels have a 3D interconnected porous network that facilitates ion diffusion, expands the electroactive surface area, and provides sufficient pathways for electron transport. Compared to conventional 2D graphene materials, GAs demonstrate excellent conductivity, larger pore volume, and enhanced mechanical strength [10, 11]. Hence, GAs significantly increase the supercapacitor performance through higher electrolyte penetration and improved electrochemical kinetics. Nonetheless, even pristine GAs are limited to the EDLC behaviour and usually achieve moderate specific capacitance values (100–300 F/g) and thus do not exhibit pseudocapacitive characteristics [6]. One approach that has been explored to overcome this limitation is heteroatom doping, through which surface functionalities and redox-active sites are elegantly incorporated [12, 13]. Doping the graphene lattice with different elements such as nitrogen, sulfur, or oxygen creates additional electronic states that enhance both capacitance and catalytic activity.

Out of the aforementioned heteroatoms that have been investigated, nitrogen represents the most investigated dopant owing to a similar atomic size to carbon, high electronegativity, and its ability to integrate into the carbon lattice in various bonding configurations [1, 6]. The doping process is known to introduce lone electron pairs and localised positive charges on adjacent carbon atoms, which is known to improve the conductivity and promote the faradaic reaction. Indeed, pyridinic nitrogen has been found to be the dominant configuration responsible for the improved oxygen reduction reaction (ORR) activity and enhanced charge storage capacity due to its localised electron-donating characteristics [2]. Additionally, nitrogen doping can also enhance the wettability of GAs and thus promote the transportation and access of ions to active sites. NGA prepared by hydrothermal treatment with ammonia has demonstrated improved conductivity, 8.4 at% N contents, and good electrochemical performance with a specific capacitance of 223 F/g and stable cycling in acidic electrolyte [14].

Building on this, a multi-gelation method was used to prepare nitrogen and sulfur co-doped graphene aerogels (N, S-MGA). Such N, S-MGAs exhibited excellent electrochemical performance, such as a specific capacitance of 486.8 F/g in 1 M KOH and a capacitance retention of 98.7% after 5000 cycles in a mixed redox electrolyte. Through the multi-gelation strategy, the density and interconnectivity of the aerogel were enhanced, which had been one of the main challenges of ultralight functionalized GAs due to the intended low tap density and poor mechanical strength [1]. In addition, the combined nitrogen and sulfur doping promotes redox activity due to their synergistic pseudocapacitive effects.

This review provides a systematic assessment of NGAs, focusing on how nitrogen doping influences their structural, electrical, and electrochemical properties. This paper summarises recent experimental studies and highlights the critical roles of nitrogen configuration, doping level, and the synthesis strategy in the design of GAs for supercapacitors. The work presented in this article adds to the increasing understanding of how to optimise heteroatom-doped carbon nanomaterials and demonstrates the high performance, scalability, cost-effectiveness, and environmental compatibility of the nitrogen-doped 3D graphene frameworks as SC electrodes.

2 | Fundamentals of Supercapacitors

In a standard capacitor configuration, electrostatic energy is stored between two metal plates separated by a thin insulator. The capacitance (C) is given by the equation:

$$C = \frac{A\,\varepsilon_o \varepsilon_r}{d}$$

where A is the surface area of the plates, d is the distance between the plates, ε_o is the permittivity of free space, and ε_r is the relative permittivity of the dielectric [15–17]. Normal capacitors have very low d (1 μm) and Various energy storage dev (1 m^2), which limits the charge storage abilities. To solve this issue, SCs were engineered to minimise d and maximise A for effective energy storage in a relatively small volume. A schematic illustration of the conventional SC configuration shows an ion-accessible separator sandwiched between two electrodes, all immersed in an electrolyte. Under an applied voltage, ions from the electrolyte move into the pores of the electrodes and accumulate at the interface, forming electric double layers (EDLs) with an incredibly small separation distance (~1 nm). SC electrodes are mostly based on activated carbon materials, possessing 1000–2000 m^2/g specific surface area, accounting for their high capacitance. A normal capacitor retains roughly 0.003 F, whereas an SC is capable of storing about 50 F, which is significantly higher.

SCs possess many advantages, such as a much higher power and energy density than conventional capacitors, excellent cycling life (up to 1 million cycles), and good stability under extreme temperature conditions, even as low as −40°C [15, 17–19]. The equivalent series resistance (ESR) is also low, typically ranging from 100 μΩ to 1 mΩ, allowing instantaneous power transfer without heat generation. Compared to SCs, batteries usually have an ESR in the 100 mΩ range [20]. According to Végvári (2019), a battery is capable of emitting 1000 W of heat when a current of 100 A is applied, but comparatively, an EDLC would emit just 10 W under similar conditions. SCs further have lower voltage drops, which means that they will deliver a better output voltage at any required load. For example, a 10 A SC can be fully charged in

20 s and a 100 A SC in 2 s. Such charge rates are impossible to achieve with batteries. A Ragone plot that visually compares the performance of different energy storage technologies is provided in Figure 1 [21]. Conventional capacitors feature high power but low energy density, and batteries feature high energy density but low power, SCs are a hybrid between the two. Due to their low ESR, the charging of SCs can be done very quickly and at modest voltages with an almost linear charging curve.

2.1 | Classifications of Supercapacitors

On the basis of their structure and working mechanisms, SCs can be divided into three types: electric double-layer capacitors, pseudocapacitors, and hybrid supercapacitors [22–24]. Particularly, this paper will only deal with the EDLCs, which are the basis of the present research.

2.1.1 | Electric Double-Layer Capacitors

The separation of charges at the electrode-electrolyte interface, which does not involve a chemical reaction, is what allows EDLCs to store energy [25, 26]. These devices utilise porous electrodes and ion-permeable separators that allow ion movement while preventing short circuits. Energy storage is dependent on both the electroactive surface area of the electrodes and the structure of the device. Optimising pore size to correspond with the size of solvated electrolyte ions enhances ion accessibility and hence increases specific capacitance [27]. Within EDLC, electrolytes play an essential role in the performance and are generally classified into three main categories: aqueous, organic solvents, and room-temperature ionic liquids (RTILs). While aqueous electrolytes have high permittivity and low ESR, they are limited by a small electrochemical stability window (~1 V). Going beyond this limit will lead to water splitting, which in turn decreases energy density. While employing organic solvents (e.g., acetonitrile-based systems) enables the use of higher voltages (up to 2.5 V) and better energy density, safety problems, including flammability and toxicity, are observed. RTILs offer an alternative with high electrochemical stability windows, low volatility, and improved thermal stability, which allows them to operate in different environments [28–31].

The electrical double layer has been modeled via several approaches. The earliest, the Helmholtz model (1853), conceptualizes the EDL as two rigid layers of opposite charge in infinitesimal separation. Yet, the details of ion mobility as well as thermal motion were neglected [28, 32]. Later, macro-scale theories of the EDL, introduced by Gouy (1909) and Chapman (1913), incorporated ion diffusion and thermal energy, establishing a model with the concept of a diffuse layer [33]. The Gouy-Chapman model predicts that ion concentrations near a charged electrode surface increase indefinitely with surface potential. This unrealistic expectation arises from the oversight of ion-ion interactions in the mean-field approximation. Stern (1924) presented an enhanced model that integrates the Helmholtz and Gouy-Chapman frameworks to overcome these constraints. It presents two separate regions: the Inner Helmholtz Plane (IHP), where ions are attached to the electrode surface, and the Outer Helmholtz Plane (OHP), where solvated ions diffuse gradually into the bulk. Whereas the Stern model incorporated finite ion sizes and adsorption effects, the model will be more appropriate for high ionic strength systems [34, 35]. However, this model is a simplification that overlooks or neglects multilayer adsorption and hydration phenomena. Molecular dynamics simulations can take such factors into consideration, and thus, modern approaches can also model more realistic EDL [36–38]. Compared with batteries, EDLCs can reach a power density of 15 kW/kg (one order of magnitude higher than the 1 kW/kg of batteries) and a cycle life of over one million cycles [39–41]. The energy and power density are mathematically represented as:

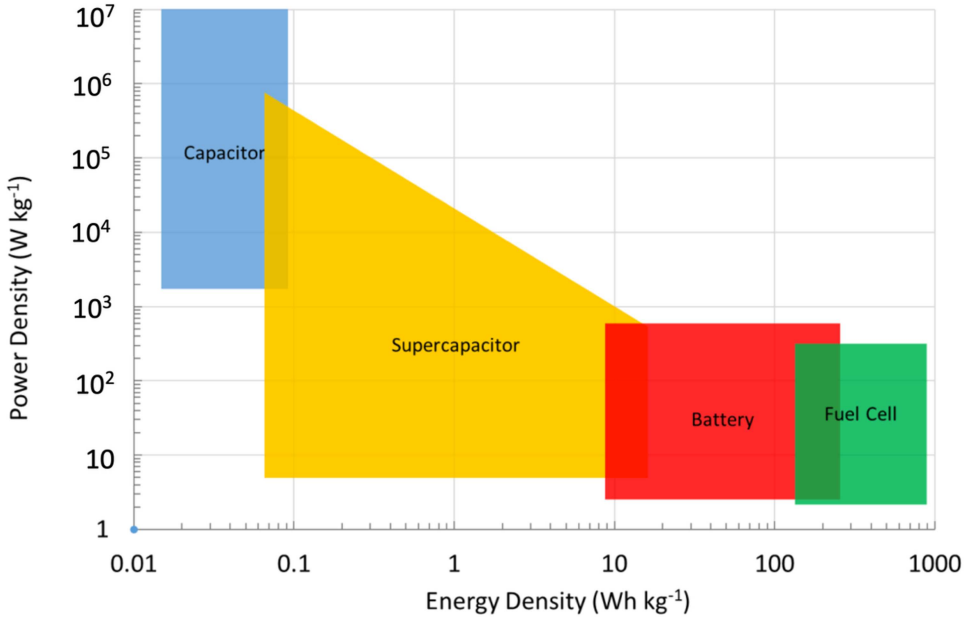

FIGURE 1 | Ragone plot for voperatingarious energy storage devices. Reproduced under the terms of the CC BY-NC-SA 4.0 license [21]. © 2017, The Author, University of Surrey.

$$E = \frac{1}{2} C_T V^2$$

$$P = \frac{V^2}{4R}$$

Where C_T is the total capacitance, and R is the ESR. Electrodes, electrolytes, separators, and current collectors all contribute to ESR [28]. At low electrolyte concentrations, it is still the Stern layer that accounts for most of the capacitance. As ionic strength increases, ion diffusion becomes the controlling factor, influencing the resistance and energy density. To make C_T better, both capacitance contributions from both electrodes need to be increased.

2.1.2 | *Pseudocapacitors*

In contrast to EDLCs, energy in pseudocapacitors is stored through Faradaic processes that involve electron transfer and redox reactions [42]. These reactions take place at the electrode-electrolyte interface and include underpotential deposition, surface redox reactions, and ion intercalation mechanisms [43]. Among these, underpotential deposition is not widely used due to limited voltage windows and high-cost materials [44]. More frequently, charge transfer at the electrode surface is reversible and can be described as a surface redox process. Pseudocapacitive behaviour often results in nearly linear profiles in CV and GCD measurements due to the rapid and reversible charge transfer facilitated by Faradaic reactions. Most of the intrinsic pseudocapacitive materials (i.e., RuO_2 and MnO_2 show rapid and reversible redox behaviour resulting from more than one oxidation state, leading to the fast transport of redox ions [45]. Hence, the following equation shows a sample reaction in the context:

$$MnO_2 + xA^+ + xe^- \leftrightarrow A_xMnO_2 (A \text{ is an alkali metal cation})$$

Ion intercalation, which is achieved by ions entering the lattice of the electrode material, is known to have faster energy storage and a longer life span. Cycling stability is much higher, and energy storage is higher as well, with materials such as MXenes. For instance, the 3D V_2O_5@PPy network prepared by hydrothermal reduction and freeze-drying reported elevated energy and power densities [46]. In yet another work, networks of carbon nanotubes and graphene fibers provided a specific capacitance and stretchability of 138 F/g and 800%, respectively [47]. Despite these advantages, pseudocapacitors typically demonstrate inferior energy densities relative to batteries, which persists in constraining their practical utility in energy storage systems.

2.1.3 | *Hybrid Supercapacitors*

Hybrid supercapacitors (HSCs), which aim to combine the high power density of EDLCs with the superior energy density of pseudocapacitors, have been developed. While EDLCs usually provide high-power output but low-energy storage, pseudocapacitors have higher energy density at the cost of power and cycling stability. Incorporating both technologies, HSCs combine the high power of EDLC-type carbon materials with the higher energy density provided by Faradaic, battery-type materials, thus delivering fast charge-discharge rates along with enhanced energy storage. This makes them appropriate for applications requiring both high power and long-term endurance [45, 48, 49]. HSCs are usually divided into symmetric and asymmetric. For symmetric HSCs, electrodes are fabricated from different materials that share the same charge-storage mechanism, while for asymmetric HSCs, the preference is for using differing electrode materials and mechanisms, which would help optimise performance. An extensively documented strategy is to substitute lithium-intercalated graphene for a carbon-containing EDLC electrode in an organic electrolyte system [50–52]. As one of the earliest HSC designs, this configuration inspired a variety of derivatives with different material combinations.

Hollow nanostructures are often adopted as structures in HSCs to enhance surface area and charge transport. As illustrative examples, double-shelled hollow structures with inner and outer shells of carbon nanotubes and carbon sulfide, respectively, constitute strong battery-type electrodes. It has been used as a positive electrode with a different negative material to assemble a device that works at 1.6 V, delivering high energy and power density and retaining 88% of its capacity after 10,000 cycles [53]. Advancements in the field showed the stabilisation of $Li_4Ti_5O_{12}$ (LTO) on carbon nanofibers through sol-gel synthesis. In conjunction with activated carbon electrodes, this configuration led to cellular-level improvements in charge-discharge rates through better interactions on the molecular level [54, 55]. It shows close to 100 percent columbic efficiency, four times greater than theoretically activated carbon capacity, and low degradation. It retains a stable potential (~1.55 V), minimises volumetric expansion, and exhibits stable performance at low temperatures down to −40 °C, with the resultant hybrid system offering capacitance of 1100–2000 F at 1.4–2.8 V operating voltages.

A comparison of structural and electrochemical features of different types of supercapacitors is provided in Table 1.

3 | Materials of Interest

In research over the years, many materials have been shown to be critical and capable materials that can be used in the construction of SCs, but in recent years, carbon-based materials have been seen to have gained increasing recognition as these materials have been identified to have significant potential and can be used for different applications in different sectors [63–65]. Many carbon-based materials, such as carbon sheets, nanotubes, and fibres, have been utilised over the years to optimise SC performance through advances in both processing techniques and material morphology. One approach taken is the mass production of 3D porous carbon nanosheets made from natural materials such as tree bark. The approach has been able to show improvements to properties, especially the specific capacitance, which reaches 340 F/g, which is an improvement and is also a green and non-toxic approach that would help in the creation of electrodes that can have high performance but at the same time are more sustainable [66]. While there is more research into different materials, the use of graphene for various applications has gained interest and more focus, which has led to this evolution.

TABLE 1 | Comparison of SC types.

Aspect	EDLC	Pseudocapacitor	HSC	Reference
Electrode materials	Carbon-based materials (e.g., activated carbon, graphene)	Metal oxides (e.g., RuO_2, MnO_2), conducting polymers (e.g., polyaniline)	Combination of EDLC and battery-type materials (e.g., carbon-based + metal oxides)	[27, 50, 51, 53, 56–60]
Working mechanism	Electrostatic charge separation at the electrode-electrolyte interface	Faradaic reactions (redox) at the electrode-electrolyte interface	Combination of electrostatic and Faradaic mechanisms	[25, 28, 45, 48, 49, 58, 61]
Advantages	High power density, long cycle life, rapid charge/discharge capability	Higher energy density than EDLC, fast kinetics, reversible redox reactions	Balanced power and energy density, improved charge/discharge rates	[40, 41, 44, 45, 53–55, 58]
Disadvantages	Low energy density compared to batteries, sensitive to electrolyte selection	Lower power density compared to EDLC, potential degradation over time	Complex design, potential stability issues under extreme conditions	[27, 28, 43, 45, 53, 54]
Energy density range	1–10 Wh/kg	10–100 Wh/kg	20–200 Wh/kg	[28, 38, 54, 58, 60, 62]

3.1 | Graphene

Graphene, the most widely studied two-dimensional carbon allotrope, is a monolayer of carbon hexagons. This material is the thinnest material known and consists of a one-atom-thick layer of carbon atoms [67]. With an extremely high specific surface area of 2630 m^2/g, it also exhibits remarkable mechanical strength (1 TPa). Although graphene is completely thin, it has very good structural strength, as well as very high thermal conductivity, about $5 \times 10^3\ Wm^{-1}K^{-1}$, and electrical conductivity of up to 10^6 S/m, making it one of the most conductive materials discovered so far [67]. The material could also be in the form of 3D nanotubes, which face a lot of issues linked with restacking, but these nanotubes can be converted into aerogels that maintain a stable 3D network without the restacking observed when they are reduced using chemical or thermal reduction [11]. This issue of restacking arises from interactions between graphene layers mediated by van der Waals forces, which are mitigated by chemical bonding during synthesis. The structure in this form is known to help improve electrical conductivity, along with providing increased charge transport between the layers, and this leads to an increase in the surface area.

Graphene oxide (GO), although having a lower surface area than pristine graphene, is frequently used in supercapacitor applications as a common constituent in building electrodes. The high capacitance of the synthesised GO is primarily due to the presence of oxygen-containing functional groups on its surface, allowing for excess charge storage. GO, while still retaining most of the properties of graphene, retains much better cyclic stability (i.e., the property of enduring charge-discharge cycles) than pristine graphene, and the low cost of the material makes this an even better candidate compared to graphene. Graphene is an excellent substrate for other active materials, such as faradic materials with pseudocapacitance properties, due to its high conductivity and mechanical property stability [11]. Figure 2 represents an overview of the various structures of graphene-based nanomaterials.

There has been an increasing number of studies that focus on the pure form of graphene as a result of its high potential, especially in the use in lithium-ion-based hybrid systems [69]. Because these materials demonstrate superior electrochemical properties, high surface area, and mechanical strength, researchers are showing increasing interest in them. That said, while these have been proven theoretically, their implementation has been slow as a result of challenges in handling the material and limitations like aggregation and restacking, which are known to have a big impact on the surface area. In order to overcome the situation, authors or researchers are said to have developed an activated form of graphene that has a surface area of 3100 m^2/g and a pore size that ranges from 0.1 to 10 nm. The material was obtained via microwave irradiation of GO, followed by KOH activation and heat treatment at 800°C (microwave-exfoliated graphite oxide, MEGO). The use of this material as a cathode while using graphite in the form of the anode in the hybrid system, being operated at 4 V, showed a specific capacitance of 266 F/g, along with an improved energy density of 53.2 Wh/kg [70].

However, Gokhale et al. (2014) have pursued an alternative direction by investigating the development of high surface area

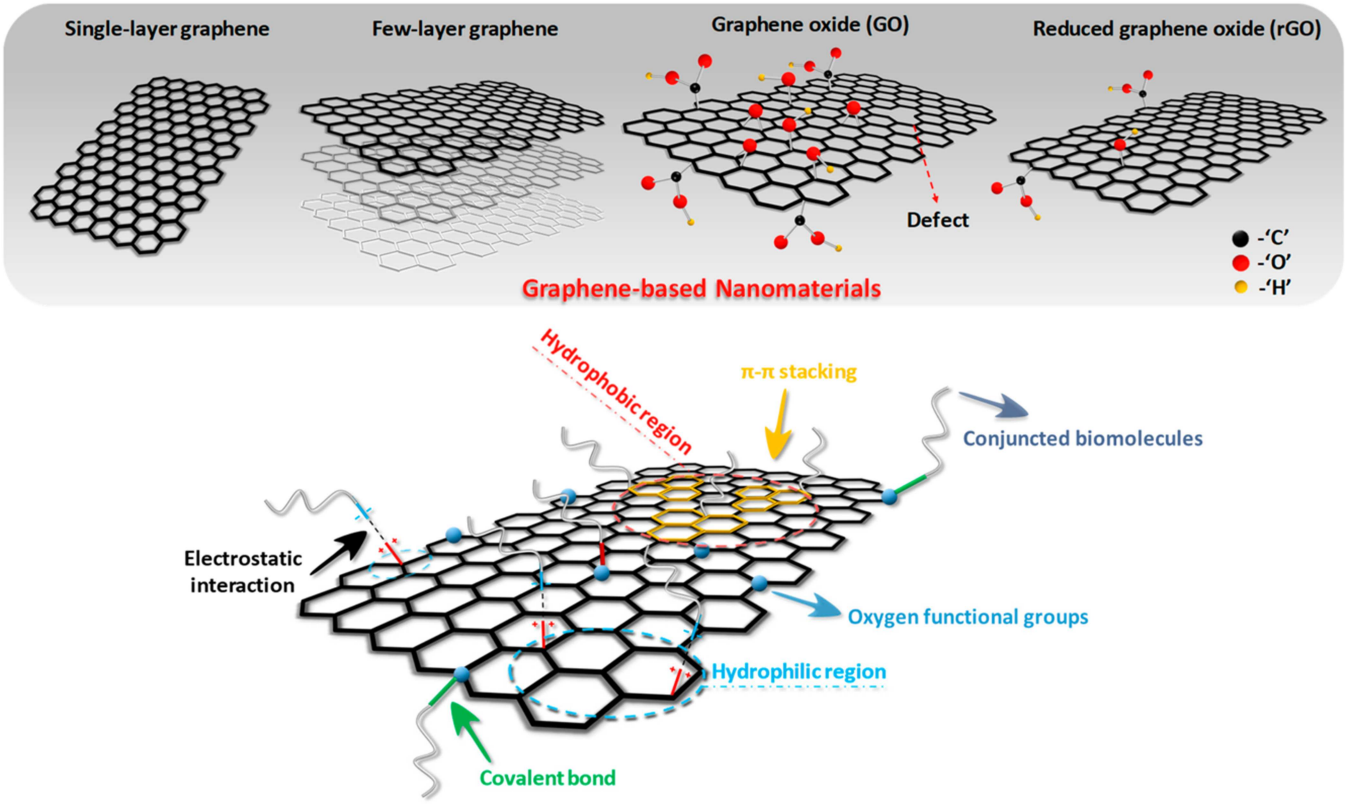

FIGURE 2 | Graphene schematic diagram. Reproduced under the terms of the CC-BY license [68]. © 2019, The Authors, published by MDPI.

and interconnectivity 3D graphene-based porous carbon materials. They adopted the pyrolysis of customized oligomers method to fabricate 3D graphene cages. Such an architecture was beneficial for fast ion conduction and increased ionic conductivity. Under standard conditions, a peak energy density of 63 Wh/kg was achieved, owing to the interconnected pores that enhance ion diffusion and charge storage [71]. From previous findings in the study, it is found that an energy density of 45 Wh/kg can be maintained with a life cycle of 5000 for the trigol-reduced GO, which would act as the negative electrode, while LTO would be the positive one [72]. In another study, the researchers developed a 3D graphene hydrogel that was to work as the negative electrode and then paired with a TiO_2-Nanobelt-Array positive electrode. The device exhibited 82 Wh/kg of energy density at a power density of 570 W/kg. It could still maintain an energy density of 21 Wh/kg at an ultra-fast charge/discharge rate of 8.4 s. The strong performance was ascribed to the rapid lithium-ion transport within the 3D graphene framework, which offered a high surface area and conductivity [73]. Defects in graphene are shown in Figure 3.

In 2015, researchers created a 3D porous graphene macrostructure (PGM) via hydrothermal treatment of GO aqueous suspension, followed by freeze-drying. This PGM showed a persistent 3D interconduction network and had a specific surface area of 373 m^2/g and a clear hierarchical structure of micro-, meso-, and macropores. As the positive electrode in an HSC, combined with an LTO/C composite used as the negative electrode, the maximum energy density was 72 Wh/kg at a power density of 650 W/kg. At 10 A/g, it also maintained 65% of its energy density after more than 1000 cycles. The PGM also exhibited an interconnected conductive network and a microporous structure, which significantly facilitated its electrochemical performance [75].

In particular, graphene-based materials have been used for their superior electrochemical performances, including high specific capacitance, energy density, and rate performance. Among these different strategies, one of the most effective is to integrate three-dimensional, macroporous structures to boost the overall performance of materials used in multiple energy storage devices. However, there are a few barriers to their real-world applications, such as materials compounding and low cycling stability. Table 2 also highlights the SC performance for some of the popular graphene-derived electrode materials.

3.2 | Graphene Aerogel

Despite the potential benefits of graphene/polymer composites, one of the major challenges encountered in combining these two materials is that the theoretical performances are often not reached, mainly due to dispersion and aggregation issues. Insufficient dispersion leads to strong van der Waals interactions, which contribute to restacking and the aggregation of graphene sheets in polymeric matrices. Hence comes the necessity to create a 3D structure of graphene that will utilize functions of its properties more extensively [10]. Among these 3D structures, such as microporous films, hydrogels, and aerogels, aerogels have shown the most potential and promise since their known porosity is approximately 90%–99%, and their density is very low, approximately 3 kg/m^3 [78–81]. In addition to this, the materials were also seen to have a lower thermal

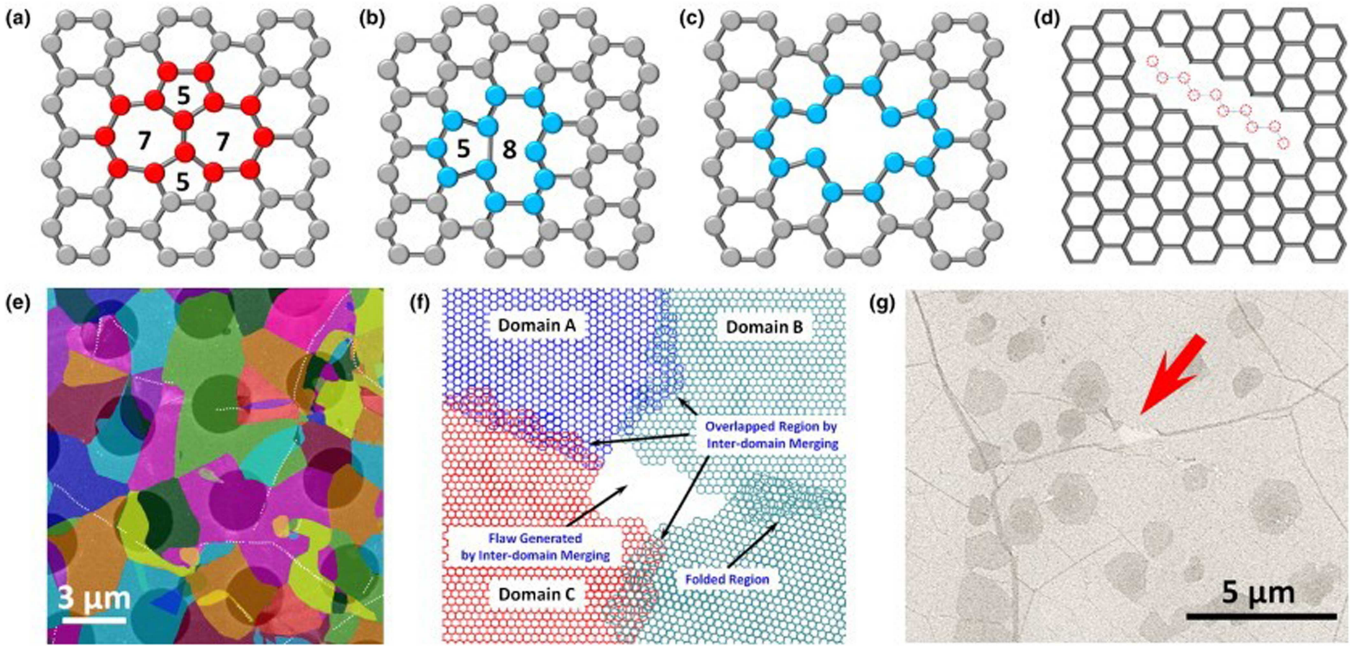

FIGURE 3 | Defects in graphene. Reproduced with permission [74]. © 2015, Elsevier Ltd.

TABLE 2 | Graphene material performance.

Material/Structure	Specific capacitance (F/g)	Energy density (Wh/kg)	Power density (W/kg)	Cycle sthe electrochemical charactability	Remarks	Study
Activated Graphene (MEGO)	266	53.2	—	—	High surface area of 3100 m^2/g with 0.1–10 nm pore size.	[70]
3D Graphene Cage	—	63	—	5000 cycles	High surface area with the 3D interconnected porous network.	[71]
3D-Graphene Hydrogel	—	82	570	—	Retained 21 Wh/kg at an 8.4-second charge/discharge rate.	[73]
3D Porous Graphene Macroform (PGM)	—	72	650	65% retention after 1000 cycles at 10 A/g	3D continuous network with abundant micro, meso, and macropores.	[75]
RGO + MnO_2 Hybrid	—	10.03	2530	69% retention after 10,000 cycles	Hybrid system using aqueous Na_2SO_4 electrolyte.	[76]
Pre-lithiated Graphene Nanosheets	168.5	61.7	222.2	74% retention after 300 cycles	Compared to graphite, graphite has superior conductivity and a high surface area.	[77]

conductivity, which is observed at ambient room temperature, in addition to lower refractive indices and a low dielectric constant. Figure 4 shows the typical procedure followed for the synthesis of GA [82].

Graphene aerogels (GAs) have a unique structure with a 3D interconnected porous network of graphene sheets. In addition to this structural configuration, the intrinsic properties of the graphene sheets also play a critical role in governing the bulk properties and performance of the aerogel. How these sheets are arranged, their size, and proportion are all key in determining the manner in which they behave as a material and what functions they are capable of carrying out. They usually present a porous structure that is generally obtained by a combination of preparation techniques, namely, hydrothermal synthesis or chemical reduction with freeze-drying or supercritical drying. These methods create a 3D network structure, which is important for energy-related materials to facilitate ion diffusion and rapid electron transport, according to Zhang et al. (2021). The study claims that hybrid aerogels developed or obtained via freeze-drying or, alternatively, via the CVD method feature increased mechanical stability and structural firmness. In addition, GAs also have between 400 and 700 m^2/g of specific surface area and are, therefore, ideally suited for use in SCs.

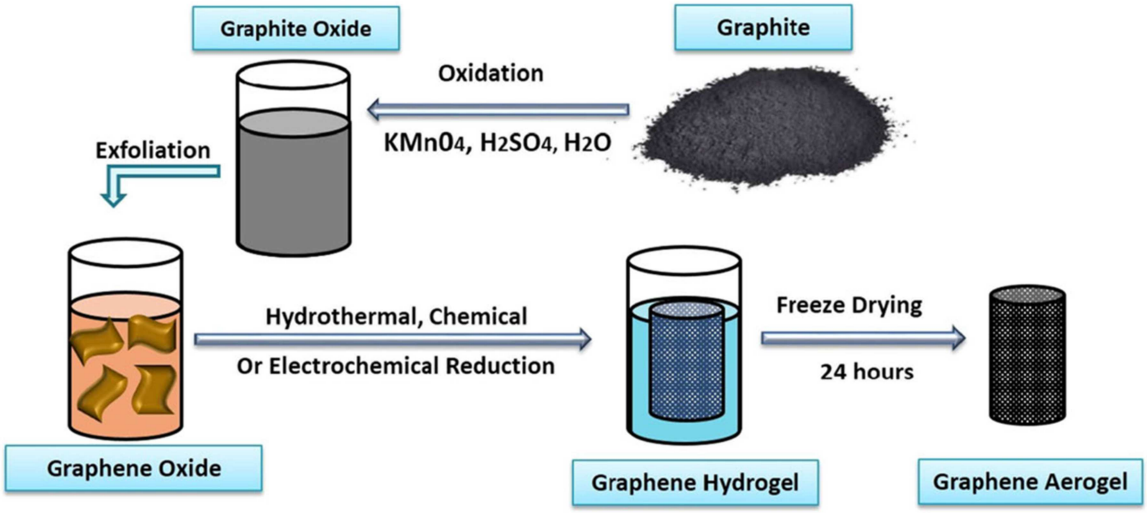

FIGURE 4 | Typical graphene aerogel synthesis. Reproduced with permission [82]. © 2017, Springer Nature.

Moreover, flexible and portable regulations are also achieved from the lightweight structure and high mechanical integrity. GAs stand out because of their unique structural properties. One of the key features that makes these a few of the lightest materials known is their ultra-low density, which is highly beneficial in other applications that require low weight, like portable and flexible energy storage devices. This is accompanied by a large surface area accessible for charge storage, attained by multiple fabrication techniques [10, 83]. Furthermore, the highly conductive network of graphene sheets ensures excellent conductivity for fast electron transport, which is essential for high-power energy storage systems. These other interesting properties of GAs, including mechanical strength and high mechanical strain-bearing capability, also enable possible practical applications for these materials [73].

The exceptional properties of GAs come with various limitations that need consideration. Their excessive porosity leads to structural instability despite being suitable for ion transport. Their brittleness shortens service life because they experience mechanical failure through cyclic stress or external loading. Furthermore, pure GAs usually encounter inhomogeneous structures after synthesis, exhibiting fluctuating mechanical and electrochemical properties. Moreover, these graphene sheets can often restack upon each other, limiting the reachable surface area and, in turn, limiting the performance. This challenge has led to investigations of strategies to improve the mechanical stability and uniformity of graphene-based aerogels. There are some drawbacks to pure GAs in terms of structure, but many efforts have been made to stabilize them through the incorporation of polymer/metal ions. The polysiloxane polymers employed are particularly beneficial because, in addition to expanding the mechanical durability of the aerogels, these cross-linked networks also restrict the aggregation of the graphene sheets, thus creating a more uniform distribution. PANI is one of the most common polymers that can be used to achieve this goal, as it increases the mechanical flexibility along with the stability of GAs. Moreover, metal ions are added to generate the so-called metal-ion–filled or open-framework aerogels, which stabilize the aerogel either by supporting weak zones directly or by making the complete structure more rigid. This integration is also fundamental for the fabrication of aerogels with improved mechanical performances and to help evaluate their supercapacitive behaviour [83, 84].

Over the years, studies have shown that polymer composites developed solely from smaller graphene sheets tend to exhibit lower mechanical properties [85, 86]. Microscopic imaging of this structure has shown that the small flakes often struggle to achieve a highly tight, uninterrupted wall structure, and that the wall surface usually has numerous joints that can overlap along defects within the structure [76]. This can lead to the conclusion that glass fibre-reinforced polymer composite is capable of showing reduced compressive modulus as well as reduced yield stress, and the GA fabricated from this would have a thickness as low as 20 μm while retaining its elasticity, and is also capable of fully recovering or retaining its initial shape even when it is subjected to nearly 80% compression strain. The graphene flakes are also responsible for the inhibiting effect on mechanical characteristics, and the aforementioned results successfully reproduce these properties across multiple investigations, thereby validating the observed alterations and performance [87, 88].

GO has several oxygen-containing functional groups, which can decrease the direct contact between graphene flakes and thus improve the structural stability of the material. To enhance performance, these functional groups can be removed during synthesis [89]. In the case of GAs, using annealing has been proven to be effective in removing oxygen groups. It is, of course, directly related to the significant enhancement of the elasticity of the material. Furthermore, annealing promotes interlayer spacing in graphene sheets, which enhances interlayer bonding and thus aids the mechanical integrity of the structure. This interlayer leads to the development of a GA material, which would have lower density but higher and improved mechanical properties, and the high-temperature treatment would also increase covalent cross-linking, along with breaking down the bond between carbon and oxygen groups, which further strengthens the carbon-carbon bonds. Covalent bonding in aerogels is responsible for the presence of structural defects, and this leads to enhanced tensile and compressive strength when compared to those GAs that do not have any covalent bonds [90].

Different configurations of GAs prepared by different synthesis methods have shown a variation in electrical conductivity. In one example, binders and cross-linkers like resorcinol were shown to be able to generate an ultra-porous graphene network in which the degree of porosity can be well controlled. To this end, GO solutions are frequently used as the basis for building the scaffold. The GAs synthesised via this technique show weak microporosity but with a remarkably high conductivity, reaching 852 S/m [91]. The porosity level observed is as high as 97.58%, and this is beneficial, as for SCs, the charges would accumulate in the pores on the surface, which would allow for improved storage. Sol-gel synthesis is another approach in which cross-linking is achieved for individual graphene sheets, followed by supercritical drying, which would help in the thermal reduction of the sheets that are needed for GA formation and have densities in the 10 mg/cm^3 range [92]. According to the study, GAs fabricated with this method show a significant improvement in electrical conductivity, about a 100-fold increase compared to physically cross-linked graphene structures. These GAs have a relatively high pore volume (2.96 cm^3/g) and a high electrical conductivity (1×10^2 S/m). Additionally, the surface area of the produced GA was notably improved (around 584 m^2/g), which corresponds to the hexagonally packed sp^2-hybridized carbon atoms, resulting in larger pores and an increased surface area. These structural characteristics are important to allow fast ion transport and to inhibit the restacking between graphene layers.

GA is a promising anode material paired with nickel oxide (NiO) as a cathode in the recent flurry of studies focusing on fabricating advanced pseudocapacitors. Such a configuration exhibited higher charge-storage capacity and significant performance improvements, especially in terms of CD cycling stability. This resulted in a capacitance of 248 mF/cm^2 for the supercapacitor at a current density of 1 mA/cm^2, making it suitable for high-performance energy storage applications [93]. The energy density for this type of GA-based supercapacitor was about 39.9 Wh/kg [94], and when MnO_2 was introduced instead of NiO, the voltage range was 0 to 2 V, which was an improvement, while it also led to increased specific energy of 23.2 Wh/kg [95]. The above characteristics make GA ideal for SC application, and even though these are theoretical, the synthesis of the material plays a critical role in the final properties.

The study by Jung et al. (2015) focuses on developing GA by making use of electrochemical exfoliation and the freeze-drying method. During the electrochemical exfoliation, sulfuric acid (H_2SO_4) and potassium hydroxide (KOH) were utilized as electrolytes. The researchers tuned the aspect ratio of graphene sheets using various concentrations of KOH (23, 30, and 37 wt %) in H_2SO_4. When using 30 wt% KOH, the ideal aspect ratio was obtained, providing large-area and thin graphene sheets with an average lateral size of 3.7 ± 1 μm and a thickness of 2.5 ± 0.1 nm. The sheets obtained were then freeze-dried at three different temperatures (−200°C, −80°C, and −20°C) to produce the aerogels. The pore size of the aerogels grew as the freezing temperature increased, as shown in the results. In particular, it showed a high BET-specific surface area of 504 m^2/g at −20°C, which was higher than that of the samples prepared at −80°C (441 m^2/g) and −200°C (315 m^2/g). The second part of the work comprised the study of graphene aerogels as SC electrodes, focusing on their electrochemical properties. Among these, the aerogel prepared at −20°C possessed the largest specific capacitance (325 F/g at a current density of 1 A/g), followed by −80°C (230 F/g) and −200°C (125 F/g). The optimized energy density of GA (45 Wh/kg) reached a new state-of-the-art value for aqueous electrolyte-based supercapacitors. Moreover, from the precise control of porous architecture, ion diffusion and electron transport were accelerated in the device, delivering high power density [96].

Tingting et al. (2016) successfully prepared nitrogen and sulfur co-doped multi-graphene aerogels (N, S-MGA) with a straightforward gel-based method. Such a dual-doping strategy is aimed at suppressing the inherent drawbacks of traditional graphene aerogels, mainly by improving the energy density and electroconductivity. The N, S-MGA electrodes displayed excellent electrochemical performance, delivering a specific capacitance of 486.8 F/g at 1 A/g and 261.8 F/g at 20 A/g in a standard electrolyte. Interestingly, in a mixed electrolyte (1 M KOH + 1 M $K_3Fe(CN)_6$), the specific capacitance was greatly elevated to 4929.4 F/g @ 2 A/g for the fabricated electrode. However, cycling stability was troubling, losing > 98.7% after 5000 charge-discharge cycles continuously. For example, it could drop to 686.7 W/kg at 1020 Wh/kg, related to 316.6 W/kg at 117.6 Wh/kg in a different measurement. Such effects highlight that the nitrogen and sulfur co-doping is extremely efficient in promoting the electrochemical performance of graphene aerogels [1]. Later, one research team created 3D porous carbon aerogels made up of N-phenyl ethanol amine, polyvinyl alcohol (PVA), and boric acid by a sol-gel method with further carbonization. The as-synthesised aerogels exhibited a super high specific surface area of 2016 m^2/g and a pore volume of 1179 cm^3/g, and the electrochemical characterization in a three-electrode arrangement showed a specific capacitance of 467 F/g at 1 A/g, in addition, the good cycling capacity where 85.7% of the initial capacitance was maintained at 20 A/g after 10,000 cycles, and even 90.9% was retained at 30 A/g, indicating their excellent cycling performance and promising application in energy storage. This yielded an energy density of 22.75 Wh/kg, indicating the appropriateness of the prepared aerogels for supercapacitor applications with high performance [97]. Their superior electrochemical properties can be attributed to the high surface area and appropriate porosity, as well as the favourable nitrogen-doped characteristics of these non-activated carbon aerogels.

In another study, Fe_2O_3/GA composite was developed by a hydrothermal process towards the design of 3D free-standing and flexible graphene-based materials for the improvement of the electrochemical behaviour of pure GAs. Herein, the study proposes a hybrid structure to configure the electrochemically active Fe_2O_3 filling uniformly at the interior of the GA framework. The electrochemical performance was evaluated in a three-electrode system in a 0.5 M Na_2SO_4 aqueous solution within a potential range of −0.8 to 0.8 V, yielding a specific capacitance result of the composite of 81.3 F/g at a current density of 1 A/g. Although the focus of this study is on composite material, it demonstrates the positive facilitator role of pure GAs as structural supports. The silk aerogel not only offered a high surface area but also an interconnected network that improved electron transport, thereby greatly contributing to the specific capacitance. This research study has used this principle of aerogel-embedding metal oxide particles into pure

GAs for better mechanical support with high electrochemical performance [98].

Another study synthesised a new class of LGN/PC aerogels with an improved three-dimensional structure via a two-step hydrothermal process to facilitate the electrochemical properties of the resulting aerogels relative to pure GAs. For a three-electrode system in 6 M KOH aqueous electrolyte, the study achieved an impressive specific capacitance of 410 F/g at a current density of 0.1 A/g [99]. Moreover, the 3D LGN/PC aerogel-based solid-state SC also exhibited outstanding cyclic stability, retaining almost no decay in performance after 5000 continuous charge-discharge cycles at a current density of 5 A/g, and the high capacitance was ascribed to the synergetic effect of porous carbon and GA structure with a large surface area for ion adsorption and efficient ion diffusion channel. In addition, the study highlighted the use of GAs as a suitable scaffold for incorporating other carbon materials to potentially improve electrochemical properties. In this sense, this strategy highlights the potential of graphene aerogels as building blocks with the versatility of additional modifications without compromising on mechanical stability and excellent electrochemical performance [99].

One study investigated the assembly of MnO_2/$MnCO_3$/rGO aerogels (MGA) using a hydrothermal approach that incorporated rod-like MnO_2 and $MnCO_3$ hybrid nanostructures with GO. Moreover, the obtained aerogels were characterized by both good electrical conductivity and strength, which was related to the supportive structure of the GA. Electrochemical testing indicated that the aerogels demonstrated an energy density of 17.8 Wh/kg over the voltage range of 0–1.6 V (with a power density of 400 W/kg). This research result showed that the aerogels modified with MnO_2 and $MnCO_3$ could enhance energy storage and have promising potential in supercapacitor applications. The results indicate that pure graphene aerogels can serve as substantial substrates to be tailored via hybridization with metal oxides to improve their energy storage properties. The graphene aerogel framework also provided increased mechanical integrity of the material, contributing to its long-term durability and mechanical stability during the 1000 charge-discharge cycles performed. These studies highlight the structural and electrochemical versatility of pure graphene aerogels when used as scaffolds for more complex materials for advanced energy storage. Due to their large surface area, excellent conductivity, and adaptable structural design, they are promising materials for coupling different active materials to achieve higher specific capacitance, energy density, and power density [100]. In addition, the significant compatibility of pure graphene aerogels with different electrolytes and composite materials indicates the broad applicability of supercapacitors using graphene aerogels as the electrode material.

We conclude that the graphene aerogels obtained from optimised electrochemical exfoliation, together with the freeze-drying method, show higher specific capacitance, energy density, and structural stability. The synergistic presence of mesopores and macropores in the aerogels facilitated fast ion transport, leading to effectiveness in supercapacitor applications.

3.3 | Heteroatom Doping of Graphene Aerogel

Heteroatom doping is an approach in which N, B, P, S, and other foreign atoms are introduced into the graphene lattice to improve its electrochemical performance. Such a modification can happen via two principal paths: substitutional doping and surface adsorption. Substitutional doping, which is the replacement of carbon atoms in the graphene lattice with different heteroatoms, would yield a thermodynamically stable structure due to the formation of covalent bonds between dopant atoms and the carbon backbone. This measure of effectiveness is largely driven by the size, electronic configuration, and electronegativity of the dopant relative to carbon. One such example is nitrogen doping, in which nitrogen atoms replace carbon atoms for improvement in the electrical conductivity (via higher charge carrier density via the presence of lone pair electrons) and modified electronic structure [101].

In contrast, surface adsorption means that heteroatoms are attached to the graphene surface instead of substituting carbon atoms. Although this method allows for flexibility during the doping process, the bonds that are formed tend to be weaker than those produced through substitutional doping. Toward this limitation, however, surface adsorption can promote the electrochemistry of graphene-based materials by providing active sites, increasing reactivity, and promoting charge transport. The heteroatom that is doped is essentially associated with the responsive performance profiles of the resultant graphene aerogel. For example, the efficient enhancement of the capacitance through nitrogen-doping could be attributed to the contribution of graphitic-N, which provides high electrical conductivity to facilitate the electron transfer, and pyridinic/pyrrolic N, contributing to pseudocapacitance. The electrochemical performance can be improved for boron-doped electrodes because boron represents electron-deficient sites, which provide sites for charge storage and enhance p-type conductivity. Phosphorus doping is attributed to different values of charge transfer kinetics due to the larger atomic size and different orbital structures of phosphorus compared to carbon, leading to some relatively strong electronic effects that change the graphene framework's electronic properties. Based on the thiophene-like structures, sulfur doping manifests the modification of the bandgap and favours the electron transfer processes, so the catalytic activity gets enhanced. Moreover, co-doping with two heteroatoms, like N-S or B-N, can produce synergetic effects to achieve superior electrochemical properties in graphene aerogels [101, 102]. This can be attributed to the creation of complementary electronic structures combined with enhanced conductivity, charge storage capabilities, and stability of doped graphene aerogels, which lead to a more effective energy storage application in combination with dopants.

The ability of nitrogen to enhance wettability and also create active sites for pseudocapacitance has been demonstrated in several studies [92]. Specifically, a 5.86 at.% N-doped graphene hydrogel synthesised via the hydrothermal method showed a specific surface area of 1500 m^2/g and a specific capacitance of 308 F/g, while another example of hydrothermally synthesised N-doped graphene with 10.13 at.% N gave a specific capacitance of 326 F/g (high cycling stability with 99.85% coulombic efficiency was maintained after 2000 cycles) [103]. In these studies, it is discussed that the capacitance characteristics can be determined by not only the total N amount but also the specific configurations of C–N bonding (such as pyridinic or graphitic N), which can enhance the wettability and electron transfer due to relatively low charge-transfer resistance [103].

The next is the application of boron doping for improving GA performance, which has also been investigated. A specific capacitance of 281 F/g was obtained in B-doped graphene structures synthesised by annealing frozen GO–boric acid composites, showing better conductivity and stability than O-doped graphene due to the presence of a higher amount of B atoms [104]. Doping with phosphorus is another method that provides encouraging results. P-doped graphene was also synthesised by annealing rGO in phosphoric acid at 220°C, showing a specific capacitance of 367 F/g at a scan rate of 5 mV/s, where the oxidised phosphorus groups are believed to contribute to the pseudocapacitance with enhanced electrochemical reactivity compared with undoped graphene [105].

Other investigations on co-doping with different heteroatoms have also been done. Abstract B, N co-doped graphene aerogel (BN-GA), with ~0.6 at.% B and 3.0 at.% N, is prepared as an additive-free monolithic composite for solid-state supercapacitors. Such material showed a capacitance of 239 F/g [106], which was several times higher than BN-doped or N-doped counterparts only, and the synergetic effect of B and N was beneficial to the energy density of 8.7 Wh/kg and power density of 1650 W/kg. However, the results obtained from a study where triply-doped rGO with 16.36 at.% O, 1.46 at.% N and 1.1 at% Cl show that the enhancement of capacitance is effectively due to the heteroatoms, as O, N, and Cl triply-doped rGO exhibit an obvious enhancement compared with the undoped rGO, which indicates that the presence of heteroatoms can introduce active sites to the graphene aerogels and enhance conductivity at the same time [107].

The GAs doped with heteroatoms possessed typical macropores in a 3D interconnected structure, which proved to be optimal for methanol oxidation and formic acid oxidation. The surface area identified by BET measurement for NGA reached 379.71 m^2/g, while undoped GA measured only 244.91 m^2/g. The nitrogen and boron atoms incorporated into the material enhance both porosity and electron and ion transport mechanisms, leading to this increased result. XPS analysis demonstrated 8 at.% nitrogen present in the doped GA while showing graphitic-N, pyridinic-N, and pyrrolic-N as its main nitrogen chemical configurations. Both frameworks in boron-doped graphene aerogel (BGA) contained similar boron contents at about 8 at.% through BC_2O and BCO_2 bonding configurations as main structural elements. Studies have shown that boron doping improves GA performance in methanol oxidation reactions (MOR) because boron atoms establish beneficial electronic conditions. The addition of nitrogen doping in GA resulted in superior CO pesticide resistance relative to standard carbon-based catalysts. Besides, due to the high content of doped GAs, the 3D porous network also provides good channels for the efficient diffusion of ions and electrons, which enables them to be suitable support materials for oxidation reactions in direct methanol fuel cell applications [12]. The performance of Pt nanocatalysts received significant improvement through doped graphene aerogels when employing them for methanol oxidation above formic acid oxidation, thus demonstrating their suitability for energy storage and conversion applications.

The SEM and TEM images from Figure 5 show the evolution of the microscopic morphology from GO to NGA, and in the SEM images, (a) GO manifests dense stacked paper-like layers with no appreciable porosity that results from oxidized graphene sheets restacked by strong van der Waals forces. On the other hand, (b) NGA has a rather open 3D porous network with crumpled inter-linked sheets showing successful aerogel formation and textural expansion by nitrogen assistance. TEM images further confirm this transition: (c) The GO presents broad, flat, few-layer sheets with wrinkles but little separation, whereas (d) the NGA exhibits thin and highly delaminated ribbon-like graphene domains with a large number of edges and low aggregation. Altogether, these images show that the nitrogen-doped aerogel process produces lighter and more open-structured graphene with improved exfoliation suitable for electrochemical applications [108].

Yu et al. (2016) synthesised sulfur and phosphorus co-doped GA for superior electrochemical performance for SC application. At 10 mV/s, the co-doped sample exhibited a specific capacitance of 438 F/g, which exceeded the capacitance levels of undoped GA at 240 F/g, P-GA at 313 F/g, and S-GA at 347 F/g, which is due to the synergistic co-doping effect, thereby enhancing the overall electrochemical performances. Moreover, SP-GA shows good rate capability with capacitance retention of 87.2% at 500 mV/s and remarkable cycling stability, with 93.4% of its capacitance retained after 10,000 cycles at the current density of 1 A/g. The research also achieved an 88.5 Wh/kg energy density, together with a 5.3 kW/kg power density based on an ionic liquid electrolyte [109]. These results indicate that phosphorus and sulfur doping at once leads to significant improvements in electrochemical capabilities, which render the modified GAs excellent options for SC use.

In one study, researchers developed a synthesis method to create graphene hydrogels by first reducing GO through hydrothermal processing before the immersion step. The hydrogel underwent immersion in a urea solution that contained 0.7 M KOH for two complete days. Under ambient conditions, the material dried before undergoing thermal treatment at 900°C in a nitrogen atmosphere. Scientists obtained NGA after washing the resulting material multiple times with deionised water [110]. In another research, it was reported that nitrogen-based compounds or functional groups react with the oxygen functional groups during the reduction process, and the final product would lead to the creation of GA that would have vacancy defects, which are known to help promote polarisation loss and enhance the electrochemical performance of the material [111]. Figure 6 presents a list of N-dopant approaches used during the synthesis of GA samples.

In Figure 6a, ethylenediamine (EDA) was used as both the nitrogen dopant and a reducing agent for GO in the synthesis of NGA, and this was based on hydrothermal self-assembly and followed up by freeze-drying [111, 112]. In Figure 6b, the ethylenediaminetetraacetic acid (EDTA) is used as the doping agent along with the chelating agent of metal ions, which is combined using the hydrothermal method with a calcination process that would eventually lead to a nickel-based NGA [113]. Figure 6c shows the use of urea as a dopant, and this is used in the preparation of graphene foam; the sample is shown to have high porosity as well as an open network formed via hydrothermal self-assembly followed by freeze-drying. In Figure 6d, the dopant used is hydrazine, while Figure 6e shows the use of dicyandiamide, and Figure 6f shows the use of ammonia [111]. EDA, hydrazine, urea, and ammonia are the most commonly used dopants for nitrogen doping in graphene-based materials

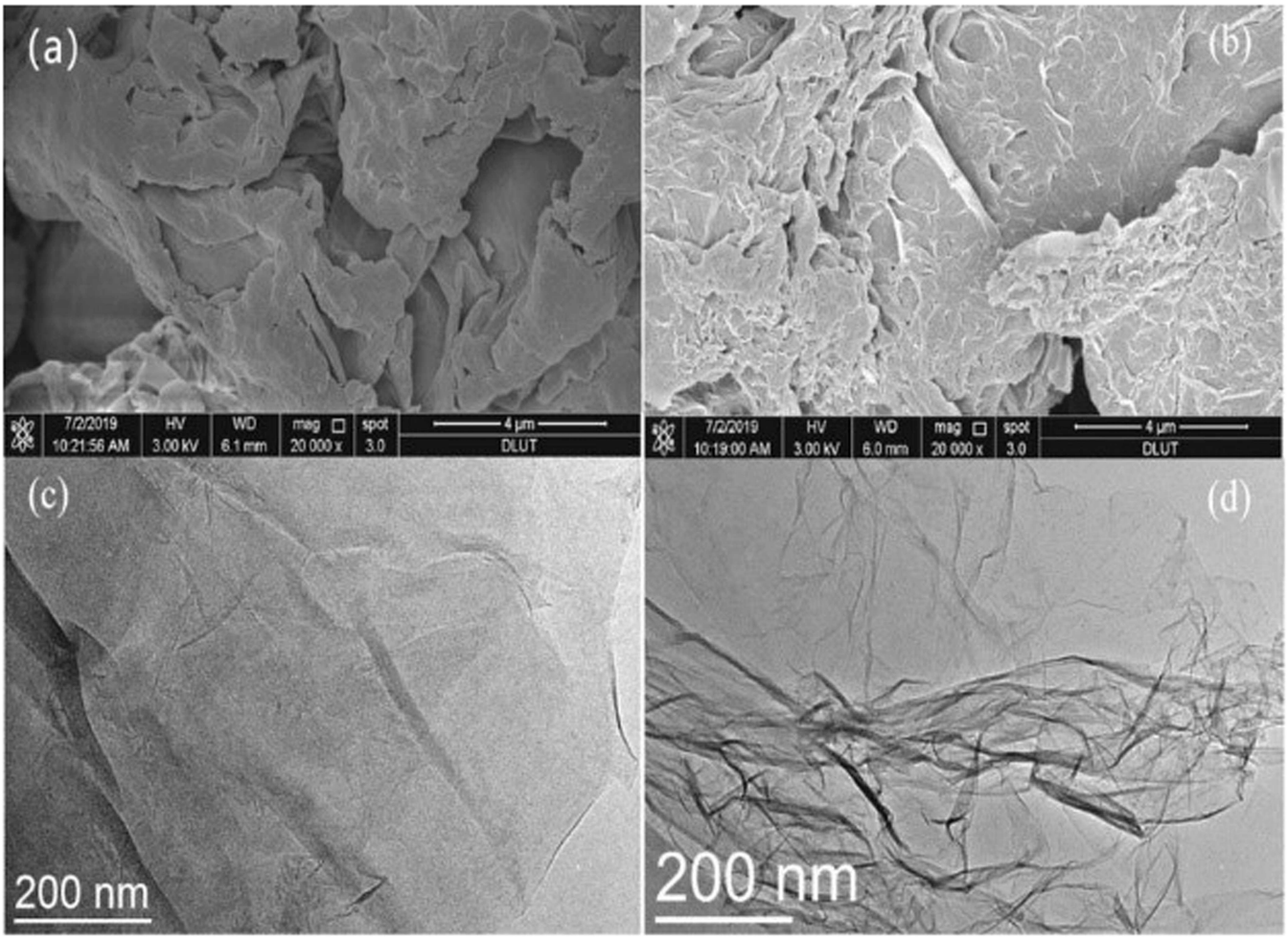

FIGURE 5 | TEM/SEM GO and NGA. Reproduced under the terms of the CC-BY license [108]. © 2020, The Authors, published by IOP Publishing Ltd.

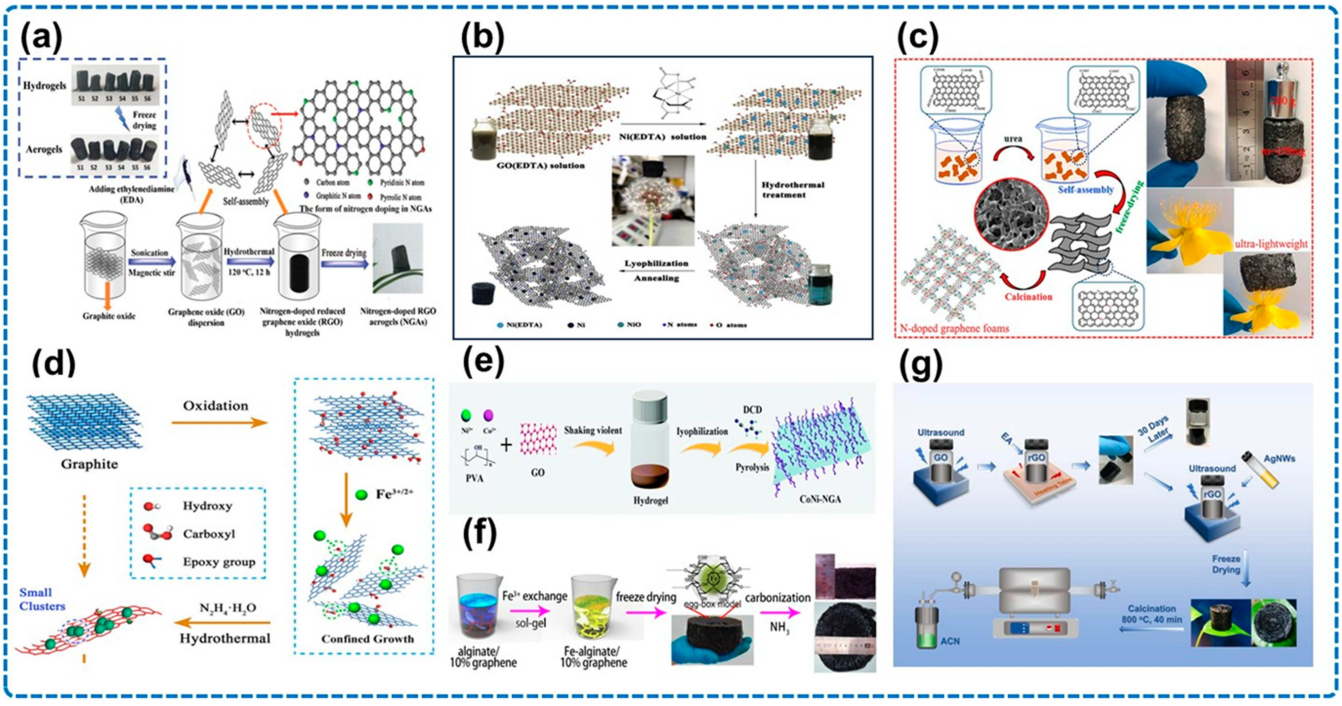

FIGURE 6 | Different selection of N dopants and illustration of aerogel samples. Reproduced with permission [111]. © 2020, Wiley-VCH GmbH.

because of the simplicity of the synthesis process and their ability to ensure that the doping effects are stable.

In the study where GO/EDA was used in a ratio ranging from 1:0 to 1:6 to explore the functionalisation degree, it was found that there was a decreasing trend for hydrogel volume with EDA content, which can be seen for differing hydrothermal duration and temperature conditions. The highest degree of temperature and duration was found to show the lowest volume levels [114]. In another study, it was found that the result N-GA had an interconnected 3D porous network, and the macropores were made of different highly wrinkled and randomly oriented graphene sheets, and the SEM images show that the interconnected porous architecture showed no obvious aggregation. The BET surface area for the NGA created was around 757 m^2/g, which is much higher compared to the traditional GA, and this was a result of the porous structure that was activated by the KOH [110]. The pores in the NGA were also continuously distributed within the range of 2 to 50 nm, which is another factor that guaranteed a higher specific surface area in the NGA.

The material analysis demonstrated that increasing scan rates from 100 to 200 mV/s created cyclic voltammetry (CV) curves with a rectangular shape that showed tilt. The tilted rectangular shape in CV curves shows high power capability and low ESR, indicating efficient charge-discharge (CD) performance. The GCD curves at different current densities are also found to be quasi-triangular and symmetrical, which is an indicator of the fact that the material shows typical EDLC behaviour along with superior CD reversibility. The specific capacitance for NGA at 0.5 A/g was as high as 175 F/g, which is similar to the specific capacitance of other elements like GAs-NaCl [110]. In another study, an NGA was developed to act as an efficient electrocatalyst in the reduction of H_2O_2, and the morphology of the structure showed that the NGA was hollow; this material was said to be ideal when it comes to direct sensing of H_2O_2 [115]. In one study that was again focused on NGA, it was found that it had a specific surface area of 830 m^2/g while the nitrogen content was high at 8.4%. This led to improvement in the electrical conductivity and wettability, and it shows a specific capacitance of 223 F/g at 0.2 A/g, along with showing high or long-term cycling stability even in sulfuric acid electrolyte, which is very corrosive. The NGA was also found to have a very high carbon dioxide uptake capacity at 1 bar and 273 K [14]. Another research shows that the capacitive conversion of charge storage was 91.7%, along with a gravimetric capacitance of 291 F/g at 1 A/g, which is quite high. In addition, the power density ranged from 650 to 23000 W/kg while the energy density ranged from 15.2 to 60.2 Wh/kg [111]. NGA based on urea was shown to have a high specific capacitance of 196.7 F/g at 1 A/g with energy density as high as 97.2 Wh/kg and a power density of around 0.9 kW/kg [116]. In addition to this, the NGA developed by this method showed 78.3% retention even after 5500 cycles at 1 A/g, showcasing good CD stability.

In another research, it was reported that a nitrogen and selenium co-doped graphene aerogel (NSeGA) was synthesised with a unique hydrothermal reduction and thermal doping approach using urea and diphenyl diselenide, which is structurally and electrochemically optimised. Its hierarchical three-dimensional network structure offers the highest BET surface area of 336.86 m^2/g among other samples tested, which indicates a larger ion-accessible surface and a lower diffusion resistance for NSeGA. Se was added to accompany N, resulting in a higher structural disorder (ID/IG = 1.15), allowing more defect sites to enhance electrochemical activity. This versatile design enables the use of both a three-electrode system and a two-electrode symmetric configuration for evaluation (NSeGAc | |NSeGA), yielding a comprehensive set of performance data from the electrochemical measurements. As a three-electrode configuration, NSeGA resulted in a remarkable specific capacitance of 302.9 F/g (1 A/g) compared with SeGA (183.9 F/g) and NGA (150.2 F/g) for single-doped samples. It also held 90.4% capacitance at 10 A/g and 94.1% after 12,000 cycles, indicating excellent rate capability and cycling stability. The capacitive symmetric supercapacitor displayed an energy density of 26.3 Wh/kg at 900 W/kg, exceeding many of the previously reported carbon systems. Its synergistic doping of N and Se led to drastically increased pseudocapacitive contributions and conductivity, while mechanical integrity and ion diffusion efficiency remained unaffected [117]. This dual-doping strategy offers an attractive route for the evolution of advanced binder-free graphene aerogel electrodes for energy storage applications.

In another work, the researchers developed a one-pot hydrothermal method for the large-scale synthesis of sandwich-layered porous nitrogen and sulphur co-doped graphene aerogels (NSGAs). GO is used as a precursor, and 2,5-dimercapto-1,3,4-thiadiazole (DMTD) is used as a bifunctional agent. DMTD serves as both a heteroatom dopant, with fascinating sulphur content up to 2.39 at.%, and a structural modifier that effectively prevents GO layers from restacking through hydrogen bonding and π–π supramolecular interactions. Electrochemical tests with a three-electrode system demonstrated that the selected NSGA-2 provided a specific capacitance of 321 F/g at 1 A/g, which is almost two times as high as that of undoped graphene aerogel. In addition, a symmetric SC device assembled with the NSGA-2 electrodes exhibited an energy density of 10.52 Wh/kg, together with a 10 kW/kg power density and outstanding cycling stability (92.8% retention after 6000 cycles) [118]. The results demonstrate that supramolecular design strategies are promising for simultaneously enhancing the structure and the electrochemical performance of graphene-based aerogels. With the combined effects of N and S co-doping as well as controlled morphologies, NSGA materials can be promising candidates for practical high-performance supercapacitor applications.

In a separate study, they reported the hybridisation of three-dimensional aerogels made from a single or bi-layered MoS_2 nanosheets with nitrogen-doped graphene aerogels (NGAs). This structure is an attempt to address the restacking limitation of MoS_2, which is commonly attributed to van der Waals forces that have adverse effects on ion transporting and electrical properties. The nitrogen-doped graphene aerogel acts as a conductive scaffold, dispersing the MoS_2 nanosheets well and creating a 3D network with high porosity and good tensile properties to facilitate electrolyte access and charge transport. A three-electrode configuration was used to assess electrochemical performance. At a current density of 1 A/g, the specific capacitance of the prepared MoS_2/N-GA hybrid aerogel was as high as 532 F/g, which was far superior to that of the individual MoS_2 nanosheets or NGAs. Furthermore, the cycling

durability is outstanding, with capacitance retention of 93.6% after 10,000 cycles at 10 A/g for the hybrid electrode. The combination of the high pseudocapacitance from MoS_2 and the high conductivity and porous structure associated with N-GAs can enhance the electrochemical properties such as capacitance, rate performance, and cycle stability [119]. These results indicate that 3D MoS_2/N-GA hybrid aerogel is also a promising electrode material for next-generation supercapacitors.

A recent study focused on presenting an environmentally sustainable method to synthesise nitrogen-doped carbon aerogels (NCAs) from carbonising alkaline peroxide mechanical pulp (APMP) fibre aerogels that have recently been saturated with rhodamine B (RB) dyes. Structurally, the precursor APMP aerogel was prepared by extracting cellulose, sol-gel transformation, and freeze-drying to create a porous three-dimensional structure. The Rhodamine B dye not only served as an adsorbate but also as a nitrogen source during the carbonisation step. The SEM analysis proved the porous structure wasn't destroyed after carbonisation, and the XPS analysis showed the nitrogen content was approximately 2.15% with principally pyridinic and pyrrolic N species. The formation of a partially carbon framework enhanced the electrical conductivity. Aerogels were first evaluated by a three-electrode system in a 6 M KOH electrolyte. The NCA showed a specific capacitance of 185 F/g at 1 A/g as compared to 155 F/g in undoped carbon aerogels at the same test condition. The reason for this enhancement was ascribed to the synergetic effect of nitrogen doping and retained porosity, which facilitates electrolyte accessibility and thus enhances the pseudocapacitive contribution [120]. Additionally, the rapid adsorption characteristics and the short diffusion pathways add to excellent electrochemical performance. This study confirms a novel and eco-efficient pathway for the carbonisation of biomass as a precursor to energy.

Arvas et al. (2021) introduced Yucel's method, presenting a new type of electrogram synthesis pathway to fabricate nitrogen-doped graphene electrodes via a one-pot, mild, and straightforward pathway, a technique that is highly pure and free of chemicals at ambient temperature. By applying a range of potentials, the process also provides a way to precisely control the incorporation of nitrogen and oxygen functional groups (e.g., $–NO_2$, –COOH, –OH) formed. These species improve the electrochemical performance by promoting surface wettability and pseudocapacitive behaviours. It yields mesoporous graphene electrodes with a morphology influenced by the applied voltage window, as validated by SEM imaging. In addition, electrochemical measurements were made using a three-electrode system with EIS and CV, as well as GCD techniques. Based on the synthesis conditions, the areal capacitance ranged from 178 mF/cm^2 (0.0178 F/cm^2) to 2034 mF/cm^2 (0.2034 F/cm^2) at 10 mA/cm^2. Due to the occurrence of catalytically active oxygen-containing functional groups, electrodes produced using narrower potential ranges displayed greater capacitance. After 1000 cycles of cyclic charge-discharge testing, stable cycling performance is observed, while the mesoporosity provides continuous accessibility to the electrolyte and helps to enhance charge storage capability further [121]. This approach offers a simple and easily adaptable way to develop electrodes for graphene supercapacitors with good electrochemical performance.

Another study reports a new strategy to synthesise nitrogen-constituted interpenetrating porous carbon/graphene (NIPCG) networks from poly(o-phenylenediamine)/N-doped graphene precursors. The end result is a structure that has a highly interconnected network with a nitrogen content of 13.1 at.% along with a material density of 1.1 g/cm^3. Such architecture allows for fast electron transport and electrolyte diffusion, resulting in excellent electrochemical performance of the material. All experiments on the electrodes were performed in a three-electrode mode. The NIPCG electrodes exhibited ultrahigh specific capacitance values of 673 F/g (gravimetric) and 760 F/cm^2 (volumetric), making them suitable for use in high mass- and volume-constrained applications. The performance is ascribed to the combined advantage of nitrogen-doping and conductivity enhancement, as well as the hierarchical porous structure that facilitates the accessibility of the electrolyte. When used as both electrodes in an asymmetric supercapacitor configuration, NIPCG as the cathode exhibited an energy density of 27.6 Wh/kg at 600 W/kg power density, outpacing numerous traditional carbon-based materials. They also offered good cycling stability. This highlights its potential for high-performance energy storage systems [116]. The findings reported here clearly highlight the benefits of creating 3D interconnected N-doped carbon-graphene networks for the development of advanced supercapacitor applications.

One study reported a novel nitrogen-doped interconnected graphene aerogel (N-IC: GA) composite loaded with ytterbium (Yb)-doped Yb_2O_3 nanoparticles, prepared in one step by the hydrothermal method. In this process, p-phenylenediamine (PPD) serves the dual functionality of a nitrogen dopant and an interconnecting agent. The resulting aerogel has a 3D porous interconnected network consisting of ultrathin graphene nanosheets (5–9 nm in thickness), providing rapid charge transport and ion diffusion pathways. A symmetric two-electrode configuration was then applied for electrochemical assessment within an aqueous electrolyte of 1 M Na_2SO_4. At a current density of 0.5 A/g, it achieved a specific capacitance of 321 F/g, and its specific capacitance retained 53.4% at 16 A/g, which proved that it had a high rate capability. The device showed an energy density of 25 Wh/kg and a capacitance retention of 98.4% after 4000 cycles, indicating excellent stability [122]. Yb_2O_3 nanoparticles are incorporated to add pseudocapacitive contributions as well as to increase the graphene framework's wettability and electrical conductivity. Nitrogen-doping and metal oxide functionalization work in a synergetic way and allow for competitive electrochemical performance. This method suggests a promising route for doping rare-earth oxides into the graphene aerogels for supercapacitor applications with high performance.

Another study reports a low-cost one-step hydrothermal route for the preparation of nitrogen–sulfur co-doped reduced graphene oxide aerogels (NS–rGOA). The method directly samples this, skipping conventional carbonisation and activation processes, to develop in situ doping and aerogel formation in one synthesis step. Of the three synthesised variants, NS-rGOA3 displayed the best performance with a high BET surface area of 412 m^2/g, well-developed microporosity, and a higher mesopore presence for accelerating ion transport and electrolyte accessibility. The electrochemical performance was characterised in a 0.5 M Na_2SO_4 aqueous electrolyte by three-electrode and

symmetric two-electrode configurations. As far as we know, NS-rGOA3 achieved the best electrochemical performance in three-electrode systems, reaching an excellent specific capacitance of up to 931 F/g at 1 A/g and still retaining as high as 391.6 F/g at 100 A/g, proving the superiority of rate capability. It even preserved 96% of its initial capacitance after 10,000 cycles at 25 A/g, indicating outstanding cyclability. Utilised in symmetric two-electrode mode, the device exhibited a high energy density of 36.56 Wh/kg and a power density of 333.2 W/kg at a cutoff voltage of 1.2 V. The aerogel showed an N/S doping ratio of 7.74, surpassing the ideal ratio of sulphide to nitride, which can also result in superior conductivity and pseudocapacitance [123].

Nazari et al. (2021) describe a nanocomposite of a mesoporous carbon nitride–graphene aerogel (MCN-GA) developed using a nano hard-templating method and covalent grafting. To fabricate MCN with a well-ordered pore structure, an SBA-15 silica template was used to synthesise MCN, and then, to improve the poor electrical conductivity of pristine MCNs, they were further combined with graphene aerogels. The hierarchical porous structure of the composite derives advantages from the scaffolded ordered mesopores of MCN and the highly conductive and interconnected three-dimensional structure of graphene aerogels. The MCN-GA electrode provided a specific capacitance of ~240 F/g at a scan rate of 5 mV/s from three-electrode electrochemical testing in 1 M H_2SO_4, significantly higher than that of pure MCN (142 F/g) and GA (174 F/g). Such enhancement in performance is due to higher electrical conductivity, more electroactive sites derived from nitrogen-rich MCN, and synergistic interaction between MCN and GA components. A symmetric two-electrode configuration (MCN-GA | | MCN-GA) enabled 10,000 cycles with > 94% capacitance retention, corresponding to specific energy density and power values of 11.6 Wh/kg and 8.0 kW/kg, respectively. We believe that the results presented in this study not only suggest the potential of structure–composition tailoring and metal-free design but also demonstrate a promising material with outstanding performance stability for supercapacitor electrodes [124].

A supercapacitor fabricated in another study adopts a new type of electrode material, which was designed following an elegant hydrothermal synthesis route, wherein 1,5-diamino-4,8-dihydroxyanthraquinone-grafted nitrogen-doped graphene aerogel (DHAQ-NGA) was employed. As for the structure, it takes advantage of the redox-active functional groups of DHAQ, such as carbonyl (C=O), hydroxyl (–OH), and amine (–NH–), which would allow faradaic reactions at both electrodes. This unique configuration again permits DHAQ-NGA to operate as both the positive and negative electrode and results in a well-matched dual-electrode system, separated by an ionic liquid electrolyte. This setup properly resolves concerns of mismatched electrode capacities as may be experienced in traditional asymmetric or symmetric systems. Electrochemical characterisation shows specific capacities of 410 and 454 C/g (positive and negative, respectively) for a major advancement in charge storage through both pseudocapacitive and double-layer mechanisms. The intramolecular hydrogen bonding in DHAQ increases the strength of the material and enhances the stability during cycling. The all-device exhibits a high energy density of 117 Wh/kg at a power density of 822 W/kg, which suggests both high energy storage and rapid charge-discharge performance. This strategy tackles the neglected subject of electrode mismatching in supercapacitors by synthesising a redox-active, bifunctional composite that effectively features both side electrodes designed for capacity and stability [125].

Another research introduced a new approach for synthesizing sulfur and nitrogen co-doped graphene aerogels (SNGA) using 5-mercapto-3-phenyl-1,3,4-thiadiazole-2(3H) thione potassium salt (BII) as both pillaring agent and dopant. BII, a vertically bicyclic molecule with a distinctive nonplanar head-to-head orientation, prevents the aggregation and restacking of graphene sheets in the hydrothermal self-assembly process. Such a structural disruption facilitates the construction of the highly porous skeleton, resulting in a specific surface area reaching a very high value of 410.2 m^2/g for SNGA4. The incorporation of sulphur in BII is also efficient due to the sophisticated molecular design, giving sulphur content of BII as high as 3.71 at.%, which was facilitated by π-π interactions and hydrogen bonding in the synthesis stage. A three-electrode system electrochemical evaluation indicated that SNGA4 produced a high specific capacitance of 399 F/g accessed at 1 A/g [126]. The device delivered an energy density of 11.36 Wh/kg when tested in a symmetrical supercapacitor configuration, and it exhibited good charge storage and energy-delivering capability. This research reveals the multifunctional roles of the pillaring agents, such as BII, that not only improve the porosity of reduced graphene oxide but also allow effective doping and enhance the electrochemical performance of the electrodes, which could be ideal when designing heteroatom-doped graphene aerogels.

NG/MnO_2 nanocomposite was synthesised in one study through a two-step method: (i) pyrolysis of polydopamine (PD) coated 316 L stainless steel at 400°C and (ii) electrochemical precipitation of MnO_2 nanoflakes. In this respect, the pyrolysis step facilitated the uniform coverage of NG layers on top of the steel substrate, mostly improving the conductivity and surface functionality of the electrode. The structures of the NG and the NG/MnO_2 composition were analysed by scanning electron microscopy (SEM) and transmission electron microscopy (TEM) to find that MnO_2 nanoflakes were homogeneously distributed on the NG surface with good vertical coherence, thus forming a compact hierarchical structure with solid NG–MnO_2 interfacial contact. Formation of birnessite-type MnO_2 was indicated by X-ray diffraction (XRD) patterns, while XPS spectra confirmed successful nitrogen doping and the presence of strong Mn–O bonding. The high ID/IG ratio in the Raman spectroscopy is ideal for electrochemical activity due to the large number of defects in the structure. BET analysis was used to quantify the accessible surface area of the particles, which shows a high specific surface area proper for ion diffusion and charge accommodation in the electrode material. Moreover, the NG-MnO_2-400 electrode has exhibited a high specific capacitance of 609.9 F/g at the 1 A/g level. The nanocomposite also displayed superior electrochemical durability, maintaining 98% of its initial capacitance after 10,000 cycles. The findings from EIS suggested low charge transfer resistance and good ionic transport. NG was proven as a highly conductive substrate to enhance the conductivity, while MnO_2 nanoflakes served as a metal exhibitor to improve the electroactivity, leading to synergistic effects for the fast redox reaction with excellent energy storage capacity. Such characteristics make NG/MnO_2-400 a viable option for a high-performance

supercapacitor electrode with long operation life and high capacitance [127].

Another research prepared a nitrogen-doped holey graphene aerogel (NHGA) via an integrated process of hydrothermal synthesis and hydrothermal exclusion, and it was successfully used as the base material for developing new SC electrodes. The structural characteristic of NHGA with a large specific BET surface area (446 m^2/g) enables increased access to the surface for ions and better penetration of the electrolyte. A low charge transfer resistance of 0.4 Ω indicates excellent electrical conductivity and interfacial charge transport behaviour for the material. The origin of these structural features is due to nitrogen doping and the holes in the graphene framework, which improve the electrochemical activity and decrease the diffusion resistance. In three-electrode mode using 6 M KOH as an electrolyte, electrochemical testing showed that NHGA delivered a specific capacitance of 318.3 F/g at a current density of 0.5 A/g, which is remarkable; specifically, an NHGA-based supercapacitor in a symmetric two-electrode configuration exhibited sustainable performance, retaining a specific capacitance of 262.5 F/g after 10,000 cycles at 2 A/g with an impressive capacitance retention of 98.4%, confirming excellent long-term cycling stability. Apart from that, the device also preserved the excellent rate capability of 96.0 F/g at an ultra-high current density of 200 A/g. The device was also assessed in a high-temperature, non-flammable ionic liquid electrolyte (EMIMTFSI-80) for high-temperature and safety-critical applications. At these specifications, the NHGA-based supercapacitor exhibited an energy density of 60.3 Wh/kg at a power density of 0.9 kW/kg [128]. Such performance was maintained over a broad operating temperature range, operating from 20 to 100°C, confirming the appropriate performance of NHGA under harsh temperature conditions and thus having a promising potential in next-generation systems.

In another work, researchers developed a 3D NGA by employing naturally occurring L-asparagine (Asn) as the nitrogen doping source, which has been found to be well-suited for electrochemical applications due to its unique 3D interconnected porous structure. Out of many doping ratios, N-GA-4 (prepared using a 4:1 mass ratio of Asn to GO) achieved the best performance as a supercapacitor electrode. After hydrothermal synthesis and subsequent freeze-drying, a unique monolithic aerogel with a hierarchical structure, providing fast ion transport and electron conductivity, was obtained. This open architecture was important to enable fast electrolyte penetration, increase the number of charge storage sites, and stabilise electrochemical performance in the presence of cycling stress. NGA-4 was also used as an electrode in three-electrode and two-electrode systems, respectively. Utilising a three-electrode system, the electrode showed a high specific capacitance of 291.6 F/g at 0.5 A/g. When tested in a symmetric configuration, the NGA-4 supercapacitor achieved a maximum energy density of 23.8 Wh/kg at a power density of 451.2 W/kg, indicating its potential for use in high-energy-density storage applications. The device exhibited remarkable cycling stability by retaining 99.3% of its initial capacitance after 80,000 cycles, outperforming most reported graphene-based or carbon-based supercapacitors. Such increased performance is attributed to the homogeneous nitrogen distribution from enhanced redox-active sites and lower resistance. N-GA-4 was optimised for supercapacitor applications, while the annealed variant (N-GA-4-900) exhibited high performance with respect to ORR. The results imply an effective design approach for the sake of development of multifunctional graphene-based materials via controlled N-doping of environmentally friendly amino acid precursors. This work delivers a scalable and cost-effective synthetic approach but also positions N-GA-4 as a promising candidate to be used as high-performance supercapacitors exhibiting both unprecedented energy density and long lifetime [129].

Another study developed boron and nitrogen co-doped holey graphene aerogels (BN-HGA) using ammonia borane as a triple-functional precursor, which acts as a boron source, nitrogen source, and reducing agent at the same time. The resultant BN-HGA possessed a large specific surface area of 249 m^2/g, as well as abundant B–N bonding motifs that created high surface polarity. Such structural characteristics led to the generation of a large number of stable redox-active sites, which were beneficial for pseudocapacitive behaviours. Further, the high hydrogen content of ammonia borane formed a reducing environment during the synthesis, which facilitated the preservation of the carbon matrix and, hence, better conductivity. In addition, the aerogel structure possessed clear hierarchical porosity, which facilitated ion diffusion across the cross-section of the electrode material and further unleashed electrochemical kinetics. BN-HGA exhibited a high specific capacitance of 456 F/g at a current density of 1 A/g in a 3-electrode system testing with sulfuric acid as the electrolyte. The BN-HGA electrodes delivered a high areal capacitance of 345 mF/cm^2 at 1 mA/cm^2 and 80% capacity retention at mA/cm^2, demonstrating excellent rate performance when integrated into an all-solid-state flexible symmetric supercapacitor. Another important benefit of its mechanical flexibility was that stable performance was observed for the bent device at various angles, which suggests the device would easily be incorporated into wearable and flexible electronic systems [130]. The synergistic combination of co-doping, integrity of conductive matrix, and well-designed hierarchical porosity had a collectively positive impact, making the BN-HGA a potential high-performance multifunctional flexible energy storage device.

The study by Zou et al. (2019) prepared a 3D nitrogen and phosphorus co-doped holey-reduced graphene oxide (NPHG) aerogel as an attractive alternative to conventional graphene cathodes for enhanced performance in lithium-ion capacitors (LICs). A traditional issue for such electrodes is that graphene nanosheets have an intrinsic tendency to restack, thereby reducing the ion-accessible surface area and limiting specific capacity. In order to do that, the researchers used a hydrothermal method to create a porous network with the incorporation of heteroatoms (nitrogen and phosphorus) into the graphene framework. The obtained NPHG material shows a hierarchically porous structure and chemical modifications, leading to greatly improved electrochemical properties. In half-cell testing, the high specific capacity of 120 mAh/g (196 F/g) for the NPHG electrode at 0.1 A/g retained 92% of the initial capacity over 1000 cycles at 1 A/g, showing excellent cycling stability. The improved performance is due to both the large electroactive surface area and the synergistic role of nitrogen and phosphorus doping that can promote electron conductivity and offer a large number of redox-active sites. Furthermore,

micropores and mesopores also promote fast ion diffusion, which is crucial for high-rate performance. As an assembled capacitor with a pre-lithiated nitrogen-doped rGO-siloxene anode (NGSil-4) as a full LIC device (NGSil-4//NPHG), a high energy density of 145.86 Wh/kg (at the power density of 200.2 W/kg) was achieved. Moreover, a high energy density of 15.35 Wh/kg was obtained after being charged at an ultrahigh power density of 14,550 W/kg [131]. The scalable and low-cost synthesis pathway enables the commercial application of this advanced cathode material as a highly competitive material for next-generation high-performance LIC, as reflected by the results in this work.

Overall, it can be observed that doping with nitrogen boosts electrochemical properties, and this makes NGA very important for the future. Thus, it is considered another material to be used in the research, and in the next sections, we look at graphene aerogel's different synthesis techniques, as the synthesis method also has an impact on the final properties of the material. A summary of recent findings on various types of NGAs and their electrochemical performance as electrode materials is shown in Table 3.

Among all dopant options, nitrogen has consistently played the most versatile and industrially appealing role. It's close in atomic size to carbon, but its higher electronegativity makes it possible for the N atom to be incorporated into pyridinic-, pyrrolic-, or graphitic-type configurations and form a lot of active sites, while retaining conductivity and even improving it. This trade-off between defect formation and electronic percolation explains why N-doped GAs exhibit not only high capacitance homogeneity but also outstanding ORR/OER activity and improved wettability [136]. Moreover, N-doping is attractive due to the use of low-cost precursors, environmentally benign synthesis methods, and good environmental and toxicological characteristics. The article also shows other doping elements used, and the comparison is presented in Table 4, which provides an overview of the differences between the most used dopants. The element boron provides additional benefits, giving rise to p-type character coupled with only a minor lattice distortion. Boron-doped structures are usually reported to be flat and exhibit stable ORR activity together with high capacitive performance, especially when they have been co-doped with nitrogen. However, good and uniform distribution of B substitution proves to be technically challenging and limits its potential for large-scale application [139].

Sulfur, on the other hand, is prone to accumulate at edges and defect sites, forming redox-active centers that enhance pseudocapacitive behavior. Recent work has shown a very good synergistic effect in N, S co-doped aerogels with higher porosity and less restacking [140], and the disadvantages of this doping are modest conductivity loss and the risk of generating insulating S-rich domains. Nevertheless, sulfur precursors are relatively cheap, and co-doping is considered to be practically doable, with standard SOx handling being sufficient for environmental regulation. Phosphorus leads to strong electron donation and interlayer space expansion, thereby promoting mass transport and exposing additional catalytic sites, but its large atomic radius can cause significant lattice strain, hindering uniform doping and potentially leading to conductivity degradation [139]. P-doping, therefore, remains largely at the research stage. Finally, fluorine creates strongly electron-withdrawing C–F linkages that promote sp^2 to sp^3 carbon on the surface, producing highly polar surfaces suitable for specialized catalytic or superhydrophobic uses, but the severe conductive loss, mechanical brittleness, and toxic fluorination chemistry, including HF-risk, make F-doping not ideal for large-scale GA-based energy devices [136].

The evidence gathered from the comparison as a whole indicates that N remains the most scalable and balanced heteroatom dopant, with boron, sulfur, and phosphorus providing more specific functional advantages, and fluorine is generally limited to niche applications.

3.4 | Role of Pyridinic and Graphitic Nitrogen in NGA Supercapacitors

After N atoms are incorporated into a carbon (Graphene) structure, they take certain bonding patterns that can be identified by standard techniques such as XPS. Graphitic N (or quaternary N) is defined to be nitrogen replacing one carbon atom within the basal plane, creating three C-N bonds in a graphitic sp^2 configuration. Pyridinic N is a 3-coordinate sp^2 nitrogen located at carbon vacancy sites or edge, which forms one lone pair and two C-N bonds to carbon, typically within six-membered ring defects. Pyrrolic N, in contrast, is a five-membered ring sp^2 nitrogen integrated in a pentagonal ring defect. These species can be distinguished by their N1s binding energies: pyridinic N at 398–399 eV, pyrrolic N at 400 eV, graphitic N at ~401 eV, and so on [141]. In addition, most N-doped carbons also contain oxidized N species (e.g., N-oxides), but here we concentrate on the intrinsic pyridinic and graphitic sites shown to exist. Even though oxidized N groups (e.g., N-oxides) are often present in N-doped carbon-based materials, the most important structural and electrochemical sites are the intrinsic pyridinic and graphitic sites.

It is important to note that both graphitic and pyridinic N atoms are usually thermodynamically stable in a carbon lattice, particularly when experiencing high-temperature treatments, whereas pyrrolic N can transform to other species upon annealing [142, 143]. Therefore, there is a tendency during many synthesis processes (especially the thermal annealing with nitrogen-rich precursors) to enhance both the attachment of pyridinic and graphitic N groups. For instance, Faisal et al. (2017) employed uric acid as a nitrogen source and reached a 9.2 at% total N with high content of pyridinic and graphitic species, using two-electrode system in an aqueous electrolyte, they demonstrated the direct benefits of these configurations on the electrochemical performance, reaching a capacitance of 230 F/g (at 1 A/g) and an energy density of 62.6 Wh/kg [144].

The electrochemical roles of the dominant N-species are quite different. Pyridinic N, which is located at edge and defect sites, donates a single p-electron to the pi-system and has a lone pair that is available for redox chemistry. Its presence leads to the introduction of highly polar functional sites that increase pseudocapacitive behavior due to ion adsorption, protonation-deprotonation, and other Faradaic processes [145, 146]. As a result, the pyridinic N is responsible for capacitance values that are higher than what would be anticipated from surface area alone. However, its effect on its electronic conductivity is low and may even lead to slight p-type behavior according to DFT

TABLE 3 | NGA performance review.

Electrode material	Specific capacitance (F/g)	Energy density (Wh/kg)	Cycling stability (%)	Cycle count	Configuration	Electorlyte	Reference
N/S-GA-2	169.4	84.5	77.2	3000	Two-electrode, [Emim]BF_4	Ionic liquid	[132]
NSeGA	302.9	26.3	94.1	12000	Three- and Two-electrode	6 M KOH	[117]
NSGA-2	321.0	10.52	92.8	6000	Three- and Two-electrode	6 M KOH	[118]
MoS_2/N-GA	532	N/A	93.6	10000	Three-electrode	6 M KOH	[119]
NCA from APMP	185	N/A	N/A	N/A	Three-electrode	6 M KOH	[120]
Yucel N-G Electrode	178–2034 mF/cm^2	N/A	N/A	1000	Three-electrode	1 M H_2SO_4	[121]
NIPCG	673	27.6	N/A	N/A	Three-electrode	1 M H_2SO_4	[116]
N-IC: GA-Yb_2O_3	321	25	98.4	4000	Two-electrode	—	[8]
Co_3O_4-ZnO/NGA	543	N/A	78.5	1000	Three-electrode	2 M KOH	[133]
NS-3DPGH-150	412.9	12.9	96.4	10000	Two-electrode	6 M KOH	[134]
NS–rGOA3	931	36.56	96	10000	Three- and Two-electrode	0.5 M Na_2SO_4	[123]
MCN-GA	240	11.6	94	10000	Three- and Two-electrode	1 M H_2SO_4	[124]
DHAQ-NGA	410–454 C	117	N/A	N/A	Dual-electrode	Ionic Liquid	[125]
SNGA4-BII	399	11.36	N/A	N/A	Three- and Two-electrode	—	[126]
NG/MnO_2-400	609.9	N/A	98	10000	Three-electrode	—	[127]
NHGA	318.3	60.3	98.4	10000	Two-electrode	Ionic liquid EMIMTFSI-8	[128]
N-GA-4 (Asn)	291.6	23.8	99.3	80000	Three- and Two-electrode	6 M KOH	[129]
BN-HGA	456	N/A	80	N/A	Three- and Flexible Supercapacitor	H_2SO_4	[130]
NPHG	196	145.86	92	1000	Half-cell and Full LIC	—	[131]
NS-MXene	495	N/A	98	6000	Three-electrode	1 M Li_2SO_4	[135]

TABLE 4 | Dopant comparison.

Dopant	Main electronic effect	Typical benefits in GAs	Key drawbacks	Scalability and safety (relative)	Specific Capacitance (F/g)	Reference
N	n-type, high defect/ active-site density	Large capacitance and ORR/ OER activity; good conductivity and wettability; widely optimised	Some loss of intrinsic sheet strength at high N; speciation control (pyridinic vs graphitic) needed	**Best:** Low-cost precursors, environmentally benign synthesis routes, and favorable biological and ecological profiles	931	[123]
B	p-type, mild lattice distortion	Preserves planarity; improves ORR, capacitive behaviour; synergistic with N	Lower active-site density; high-B uniform doping is difficult	**Good–moderate:** Requires higher temperatures and tighter process control, but no major toxicity concerns, but no major toxicity issues	308.3	[137]
S	Edge/defect localisation, redox-active	Adds faradaic sites; boosts capacitance in N,S co-doped GAs; helps prevent restacking	Slightly reduced conductivity; risk of over-doping and insulating S clusters	**Good:** Cost-effective and straightforward co-doping with N; standard SO_x emission management is sufficient at end-of-life	347	[109]
P	Strong electron donor, increases interlayer spacing	Highly active sites for ORR and charge storage; enlarged pores aid ion diffusion	Strong lattice strain; difficult homogeneous substitution; conductivity can drop if poorly controlled	**Emerging:** Effective but more complex and energy-intensive; currently limited to research-scale	313	[138]
F	Strongly withdrawing; converts $sp^2 \rightarrow sp^3$	Highly polar surface; niche electrocatalytic or superhydrophobic uses	Severe drop in conductivity; brittleness; higher cytotoxicity; HF/HF-related hazards	**Poor:** Involves hazardous chemistry, corrosion risks, and challenging process control; unsuitable for large-scale GA-based energy devices	279.8	[138]

predictions. Its agency is thus principally chemical activation rather than electronic increase; therefore, it can be particularly beneficial for pseudocapacitive reactions and catalytic reactions. Graphitic N, on the other hand, replaces itself directly into the basal plane and offers one more electron to the conjugated system, functioning as an n-type dopant. This incorporation induces a higher Fermi level and carrier density, which leads subsequently to higher electronic conductivity and higher EDLC contribution to capacitance [144]. These conductive improvements reduce electron transport pathways, allowing for faster charge-discharge processes and even better rate capability. Although graphitic N is less reactive than pyridinic N in terms of both chemical reactivity and lack of direct participation in redox reactions, it has a modulating effect on the carbon electronic structure, may enhance the accessibility of ions, and may increase interlayer distance slightly. Furthermore, attention has been drawn to the fact that quaternary N can promote surface wettability, thereby enhancing electrolyte penetration and electrochemical utilization [145, 147].

The dual benefits of nitrogen active sites in these materials arise from: (1) Faradaic pseudocapacitance created from surface redox reactions, and (2) increased conductivity aiding well double-layer charging kinetics. The former is mainly affected by pyridinic and graphitic N species, which also exhibit a synergistic effect when used together [143, 145]. These underlying mechanisms have been revealed by Density Functional Theory (DFT) calculations, with one study employing the method to determine the impact of various N-bonding on graphene's capacitance, showing that graphitic and pyridinic N enhance total capacitance by increasing quantum capacitance [146]. On the other hand, pyrrolic N tends to lead to a capacitance reduction owing to its lower contribution to the electronic density of states near the Fermi level. This difference is due to the fact that graphitic and pyridinic N can be involved in the creation of extra electronic states that can be involved in the charge storage process, while the localized pentagonal ring structure of pyrrolic N cannot provide the same benefit. DFT calculations also showed that graphitic-N doping shifts graphene's Fermi level into the conduction band (n-type doping), whereas pyridinic and pyrrolic N can induce p-type behavior, results that are in good agreement with their experimentally observed impact on conductivity [142].

These theoretical predictions are well confirmed by experimental evidence. As mentioned in one study, the synthesized graphene enriched in pyridinic and graphitic N was shown to exhibit the highest specific capacitance of 230 F/g and an energy density of ~62.6 Wh/kg, much higher than that of undoped graphene-based electrodes [144]. More recently, Gu et al. (2023) showed the distinct electrochemical roles of pyridinic and graphitic N by making use of a tunable N-doped porous carbon that is derived from 4,4′-bipyridine, which provided some form of control over configuration. The material with higher pyridinic content showed a much higher specific capacitance of 436 F/g in aqueous KOH electrolyte because of the increased pseudocapacitance, and it also retained 100% capacity over 5000 cycles. This emphasizes the ability of pyridinic N to form reversible Faradaic active sites, presumably involving a reversible redox surface group or N-OH in alkaline electrolyte. In contrast, in an ionic liquid electrolyte ($EMIMBF_4$), the carbon materials enriched in graphitic N delivered higher energy densities (up to 125.4 Wh/kg) due to better double-layer charge storage and electronic conduction behavior [145]. The lower internal resistance and more efficient electron transport were due to the graphitic N, which typically does not participate in Faradaic reactions, but which benefited electron transfer only through EDLC.

In addition to standard electrochemical measurements, in-situ/operando characterizations are beginning to uncover information about how N functional groups behave during charge–discharge. For example, operando XPS and related spectroscopic studies have shown that surfaces enriched in pyridinic/pyrrolic N can experience reversible chemical interactions with electrolyte species during cycling. These interactions are usually represented as weak redox peaks or deviations from the ideal rectangular shape in CV curves, reflecting combined non-Faradaic (EDLC) and Faradaic contributions typically associated with surface functionalities such as quinone-like moieties or protonation-deprotonation of N sites in acidic electrolytes [143]. On the contrary, graphitic N is likely to be sustained electrochemically active but chemically inactive upon cycling. Its main contribution is the enhancement of electronic conductivity, leading to lower equivalent series resistance (ESR) and faster frequency response. For example, Zhang et al. (2016) demonstrated that the bulk conductivity of graphene/Fe_3O_4 aerogel (174 $S.m^{-1}$) was tripled due to plasma treatment by introducing graphitic N as compared to undoped RGO, which in turn significantly enhanced the rate capability of the supercapacitor. The authors also reported that hydrothermal reduction alone produced N primarily as pyridinic/pyrrolic N, with little graphitic N, whereas plasma treatment generated a distinct graphitic-N XPS peak at 401 eV [141]. The plasma-doped aerogel exhibited 153% enhanced specific capacitance compared to that of the undoped baseline, which pointed out that it was crucial to obtain graphitic N in the framework for unlocking high performance with respect to electrical connectivity and effective utilization of the 3D porous structure.

In conclusion, pyridinic-N and graphitic-N are used as cooperative active sites in graphene aerogel electrodes for supercapacitors. Pyridinic N serves as an electrochemically active site, which is capable of reversible redox processes to enhance capacitance through the pseudocapacitance effect, while Graphitic N mainly promotes the electronic properties of the graphene-based materials by increasing electrical conductivity and raising the density of states in its conduction band to improve double-layer capacitance and rate capability. Simultaneous coexistence of the two types in a synergistic manner can yield ultrahigh overall capacitance and energy density, particularly in materials that combine a high-surface-area 3D framework with rich pyridinic and graphitic N content. This mechanism is corroborated by DFT studies that show increased quantum capacitance associated with these dopant-induced electronic modifications. These dopants, and in some cases the way they behave under operation, have been directly observed with advanced characterization techniques (XPS, in-situ spectroscopy), confirming their functional roles.

4 | Performance, Stability, and Scale-Up Considerations for NGA Devices

Flexible NGAs should withstand repetitive deformations like bending and compression while in operation. Owing to

graphene's intrinsic mechanical strength, these aerogels can provide high fatigue resistance; e.g., hybrid graphene aerogel sensors show consistent piezoresistive performance under loading/unloading for more than 20,000 cycles [147]. Similarly, a nitrogen-doped graphene composite aerogel demonstrated remarkable elastic and compressive properties for use in pressure sensors, with ultralong-term compressive cycle stability and sensitivity after thousands of uses. These findings show the importance of structural design strategies, such as polymer reinforcement or CNT incorporation, which can significantly preserve functionality in NGA-based devices subjected to long-term mechanical stress [148]. Nevertheless, pristine graphene aerogels remain brittle, and their highly porous structure can be plastically deformed or collapse under certain stress conditions. Accordingly, the development of a durable aerogel structure capable of surviving mechanical fatigue and microfracture is required so that these materials can endure in the long term [3].

For wearable or flexible power sources, NGA-based electrodes should be able to withstand the repetitive charging-discharging process, and nitrogen doping can provide more active sites and higher conductivity, thereby improving electrochemical performance. In past studies, it has been demonstrated that NGAs have high capacitance with stable cycle stability in long-term cycling. For example, an NGA electrode showed higher capacitive properties and kept steady capacity during long-term charge/discharge in H_2SO_4 electrolyte. At the practical level, NGA-SSCs exhibit about 80%–90% of their initial capacitance after several thousand cycles, indicating excellent cyclic stability. However, severe operating conditions (e.g., a high-current cycle or temperature changes) may reduce its performance due to the decomposition of an electrolyte or structural instability, and hence, cautious device encapsulation and heat dissipation are part of the NGA device life history in order to maintain such performance levels under real operating conditions [14].

Any wearable device has to be compatible with direct or occasional skin exposure. In general, graphene-based materials are considered biocompatible for skin-mounted sensors but can be potentially hazardous when reduced to nanoscale dimensions. Notably, many studies indicate that nitrogen doping can improve the biocompatibility of graphene or its derivatives. In a 2024 study, it was reported that substantially reduced oxidative stress and cytotoxicity for N-doped graphene were much lower than that of pristine GO in vitro and in vivo assays, and it was found that the N-doped graphene induced very low levels of inflammation and apoptosis, suggesting that it might be useful for biomedical or on-skin applications [149]. However, despite this promising result, some cases have been documented in which direct contact with graphene has caused mild skin irritation in an occupational setting. Therefore, it is also important to ensure that NGA-based wearable devices are encapsulated or coated with biocompatible layers to avoid potential skin irritation and the release of nanoparticles [150]. Toxicological assessments of NGAs are continuing, and although they appear to be relatively low risk at present, long-term studies are still needed to determine their safety based on long-term use.

Understanding how NGA devices fail is also a key factor in safe operation. One common failure mode is mechanical damage to the material, which can reduce structural integrity and potentially cause graphene particle release. The open structure of NGAs may cause the network to collapse when overstressed, which leads to a rapid decrease in conductivity or sensing performance. To alleviate this, devices are designed with strain limits and strong encapsulation in such a way that the aerogel remains contained upon fracture. Another issue with energy-storage devices is overheating or shorting, and although carbon aerogels are nonreactive and nontoxic under ambient conditions, they may become hot if an internal short circuit occurs in a flexible battery or supercapacitor [3]. The electrodes themselves of NGA are stable even if the temperature becomes high, but it is possible that they will be oxidized and produce carbonaceous dust and nitrogen oxides, because of the existence of nitrogen content. Based on this, thermal management and circuit protection are used to avoid thermal runaway. In summary, for the safe deployment of NGA-based wearable devices, a combination of system-level protection strategies, such as encapsulation, thermal management, and circuit protection, must be supported alongside materials optimization strategies, such as emphasizing composite reinforcement to ensure long-term mechanical integrity and reduce health and safety risks.

There are several challenges in migrating NGA devices from a lab prototype to large-scale industrial production, such as the uniformity of materials, which highlights the challenges of nitrogen doping and pore structure consistency across large aerogel batches, which are non-trivial [14]. High N content and high BET surface area are hard to achieve at the same time, and one may hinder the other. To obtain NGA with reproducible properties, tight control over sol-gel chemistry or CVD processing conditions is demanded, and the device's performance can vary even with minor differences in the doping levels and/or pore size distribution.

Laboratory NGA production typically uses self-assembly techniques (e.g., hydrothermal, chemical reduction) followed by freeze-drying or supercritical drying, which can be expensive and difficult to scale up, and given these cost-intensive, complex processes, it appears uneconomical on an industrial scale. In addition, producing high-quality graphene in bulk is itself costly, and doping it (depending on the doping source) is expensive; thus, this is a well-known limitation to the extensive commercialization of graphene-based SCs and sensors. Cheaper routes, such as ambient-pressure drying or 3D-printed GAs, are being explored to increase throughput. For flexible electronics, NGA materials have to be compatible with polymeric or textile substrates, but it is not easy to have strong adhesion and compatibility between a brittle aerogel and a soft substrate [3]. Differences in mechanical properties between these two can result in delamination or cracking upon bending the device, and one solution is to add polymers or binders to the NGA (composites) to impart flexibility and improve bonding [148]. A further problem is maintaining a stable electrical contact. In large-scale integration, there must be reliable methods for patterning or attaching NGA electrodes without sacrificing their high specific surface area or structural integrity.

All of these scale-up challenges–including material uniformity, cost, and integration are still an active area of research. For example, there are ongoing efforts to strengthen NGAs through tailored formulations (e.g., adding cross-linkers or secondary nanomaterials) that impart greater mechanical strength and improve the roll-to-roll manufacturing of NGA-based inks. Solving these problems is key to getting NGA-based wearable devices out of the lab and into the commercial space.

5 | Electrolytes and Their Influence on NGA Performance

NGAs exhibit electrolyte-dependent features, since ion size, ionic conduction, viscosity, and voltage stability in hierarchical pore networks directly influence the charge storage. In aqueous KOH, performance is limited by the very high ionic conductivity and low viscosity, which allow rapid mobility of K^+ and OH^- through the aerogel pores [151]. Given the small size of these ions, they can reach most micropores; hence, NGAs show very high specific capacitance, with reported values up to 346 F/g in KOH and approximately 321 F/g retained after 2000 cycles [152]. Nitrogen sites additionally improve wettability and redox-active pseudocapacitance that could avoid structural collapse and preserve its electrochemical stability upon long-term cycling [153]. The most significant drawback of aqueous electrolytes is the relatively narrow voltage window of water (~1.2 V) that has limited energy density despite high capacitance ($E = \frac{1}{2}CV^2$). Nevertheless, aqueous NGAs are still interesting candidates when benefits such as high power, fast charge–discharge ability, and stable cycling are required, with degradation observed only close to the electrochemical limits of water, where some carbon corrosion may take place. Well-designed N-doped aerogels commonly circumvent harsh damage losslessly.

For organic electrolytes such as 1 M $TEABF_4$ in acetonitrile, the main advantage is the very broad voltage window of 2.7–3.0 V, with energy density twice that of aqueous systems [151]. Nevertheless, the ion mobility is lower as the ACN-based electrolytes are more viscous and less conductive than KOH, leading to higher internal resistance and reduced rate performance. Organic ions, in fact, have a size much larger than K^+; TEA^+, for instance, has an equivalent diameter of 0.68 nm, which prevents it from entering the smallest micropores. As a result, the capacitance is rather low (100–150 F/g), and a porous carbon electrode gives 130 F/g at 1 A/g. Organic systems do lose capacitance but make up for it with high energy, such that, e.g., a carbon device operating at 3.0 V could reach 55 Wh/kg. Cycling stability is also strong, with 85% of the specific capacitance retained after 10,000 cycles in $TEABF_4$/AN [153]. In NGAs with multimodal porosity, mesopores can provide pathways for the transport of bulky ions and effectively bridge the gap between aqueous and organic systems, while nitrogen doping can further increase polarity and improve ion anchoring, mitigating the penalty associated with large organic ions.

Ionic liquids (ILs) electrolytes, particularly $EMIMBF_4$, provide the largest voltage window of 3.5–4 V, giving rise to very high energy densities, often exceeding 100 Wh/kg. On the other hand, ILs have considerably greater viscosity and lower ionic conductivity than other electrolytes [151], which slows down ion transport and restrains high-rate performance. Ion size is relevant again, with $EMIM^+$ ($\approx$0.7 nm) and BF_4^- ($\approx$0.48 nm) bearing difficulties passing through micropores, making hierarchical meso-macroporosity essential for optimal performance. Despite these limitations, NGA in pure ILs delivers decent capacitances, typically 150–210 F/g, with reports of up to 212 F/g and 182 F/g in N/S-co-doped aerogels. Due to the high operating voltage, energy densities of 100–117 Wh/kg at ~1 kW/kg are attainable, and IL-based NGA devices have good cycling stability, ~90% retention after 3000 cycles [153]. The solvent-free nature of ILs inhibits common degradation routes related to electrolyte decomposition, enabling their safe high-voltage operation.

Across all electrolyte classes, three general principles consistently emerge, and the first of this is that ion size has to match pore size: small K^+/OH^- ions make use of microporosity to its fullest extent, while bulky TEA^+ or $EMIM^+$ need mesopores; this is illustrated by a hierarchical carbon/graphene electrode where KOH achieved 303.8 F/g vs 280.0 F/g for an IL, which is in line with structural optimizations reducing ion-size penalties. Second, viscosity determines power performance, as the ion transport in aqueous KOH is fast, ACN-based organics exhibit intermediate behaviour, while very viscous ILs result in the least power. Third, the nitrogen doping is also beneficial universally, resulting in improved wetting ability, conductivity, and pseudocapacitive ion binding, which increases the capacitance in all electrolytes. Taken together, the literature reveals that the choice of electrolytes controls the trade-off between capacitive power and energy density, while nitrogen-doping consistently stands out in all aqueous, organic, and ionic-liquid systems.

6 | Synthesis Techniques

Since micromechanical cleavage produced the highest-quality graphene with the fewest flaws, it was initially the most widely utilised method for graphene production [154]. The Scotch tape method, so named because it uses adhesive tape in the exfoliation process, was devised in response to the technique's limitations and in an effort to find alternative approaches. As seen in Figure 7, a wide variety of methods have been used over time and may be categorised as either top-down or bottom-up methods [155, 156].

The former method is said to be a process that starts with fragmenting bigger precursor materials that would lead to the smaller graphene structures. A combination of scalability and high-quality production with minimal defects makes this approach highly desirable. That said, this approach does have its own challenges, specifically linked to its ability to ensure consistent characteristics, obtain optimal yields, and, the biggest of them all, reliance on resources like graphite producers, which are very limited. The bottom-down approach, on the other hand, is known to use other carbon sources in order to synthesise graphene, and these would involve developing from an atomic-sized precursor, which leads to a defect-free material, and these are known to have a higher surface area. These processes are costly compared to the top-down approach, and the steps required for the conversion of the process are also very sophisticated [157].

From these two approaches, there have been different techniques introduced for the synthesis of GAs, and the most widely popular techniques are chemical reduction and hydrothermal reduction, which are attributed to the approaches' facile synthetic route in addition to the increased control the chemical reduction provides in controlling the pore morphology [10, 158, 159]. The GAs are mostly developed from the GO precursor through a reduction process, and the GA's overall performance would depend on the dispersion of graphene in the substrate. In addition to this, there are many techniques that use the modification of the covalent and non-covalent bond between the

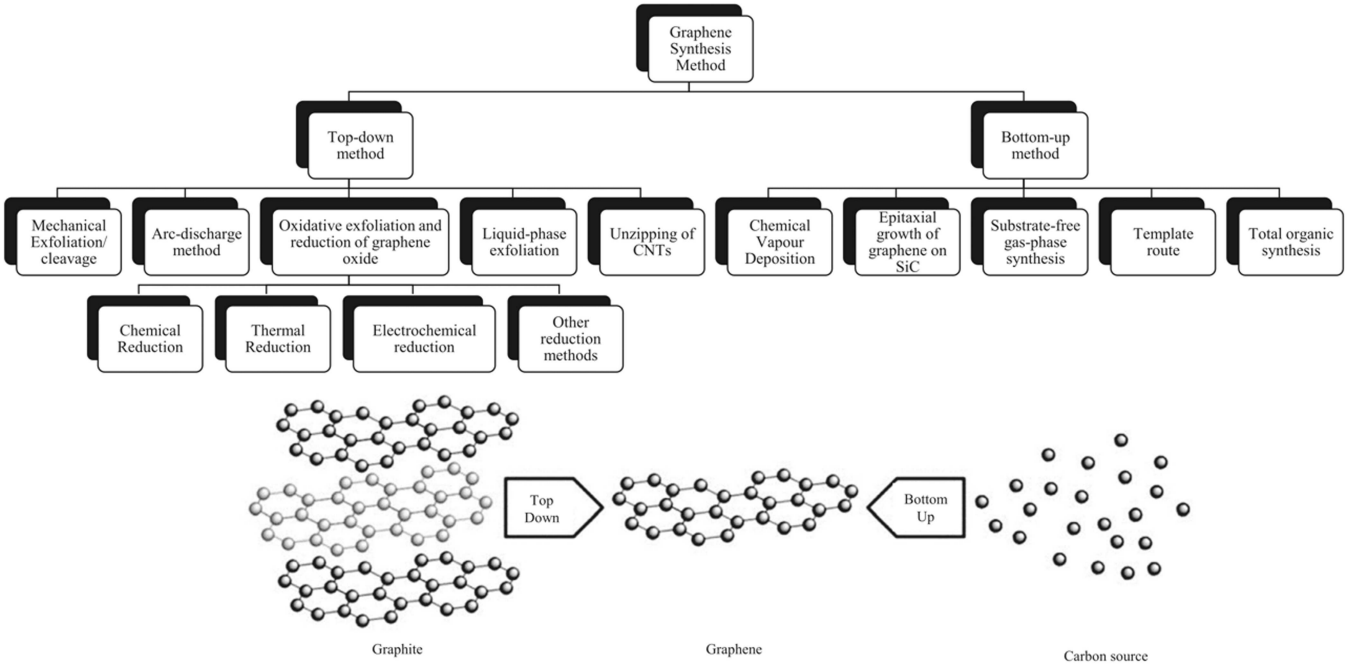

FIGURE 7 | Graphene synthesis method. Reproduced under the terms of the CC-BY license [3]. © 2024, The Authors, published by Elsevier.

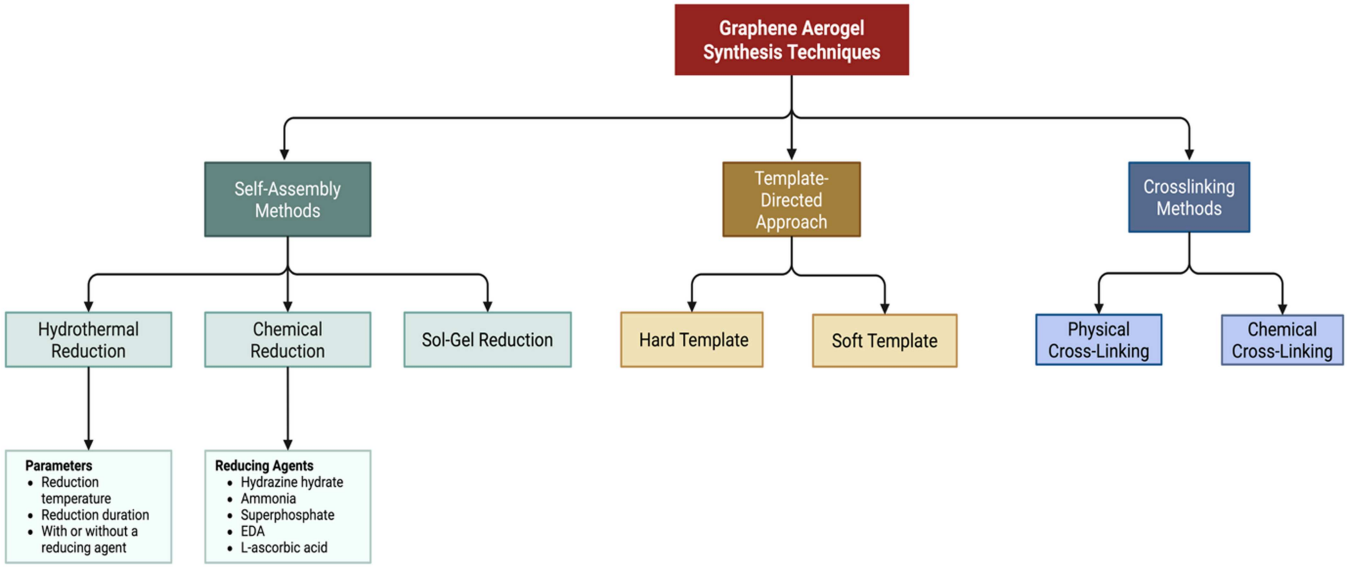

FIGURE 8 | GA synthesis methods. Created by the authors using bioRender.

polymer and GO matrix, and then this mixture is subjected to ultrasonic dispersion, which would help to break down van der Waals forces that cause aggregation, thus improving both structural quality and material performance [78]. That said, of the different techniques that are highlighted in Figure 8, the hydrothermal reduction and chemical reduction techniques are most preferred, which has been attributed to the low cost and production scalability of these techniques. Due to the benefits mentioned before, this research will make use of hydrothermal reduction, and this section will focus on that specific technique.

In recent years, NGAs have been prepared by a wide variety of synthetic routes, most commonly adapting wet-chemical or self-assembly methods originally developed for the fabrication of pure GA to incorporate the nitrogen source. For instance, a typical approach on a lab scale would be the hydrothermal self-assembly reduction of GO by using N-rich precursors. For example, Chen et al. (2021) employed a one-pot hydrothermal strategy involving GO and urea phosphate to create a hierarchically porous NDGA (referred to as UPGA). Urea phosphate acts as both the reducing agent and the nitrogen source, giving rise to a 3D aerogel with N-functional groups homogeneously distributed throughout the material. At 1 A/g, the UPGA achieved a remarkable 196.7 F/g and excellent ionic-liquid energy density (97.2 Wh/kg at 0.9 kW/kg). Cycling retention after 5500 cycles was 78%. It shows that in-situ doping at the same time as GO reduction can generate NGA with high capacitance; however, the approach uses serial autoclaves and later freeze-

drying, which are both time and energy-consuming processes that limit large-scale throughput [3, 160]. These hydrothermal routes are tunable by selecting the amine precursor; for example, the addition of ethylenediamine (EDA) or dicyandiamide during the reduction process gives pyrrolic-/graphitic-N and excess porosity. Note that in most cases, the electrochemical performance is indicative of both high surface area and pseudo-capacitance deriving from N-sites. Depending on precursor type and process parameters, some N-doped 3D GAs were noted to achieve outstanding specific capacitances of up to 346 F/g or ~315 F/g in aqueous solutions, as seen in a recent review. Yet, reproducibly creating these structures at scale is not trivial; the hydrothermal step is often restricted by temperatures above 100°C and hours-long reactions in autoclaves, with only grams produced per batch. Secondly, large-scale freeze-drying of these gels (to retain the aerogel porous structure) is costly and time-consuming. While these methods are impressive in the lab, they will have scaling barriers unless continuous hydrothermal reactors or new drying methods (spray freeze-drying, etc.) are used [3, 111].

Feng et al. (2021) used a hydrothermal self-assembly method with urea as a nitrogen source and foaming agent to prepare urea-based N-GA. The GO and urea were dissolved in water in a 1:1 ratio, and they were then placed in a Teflon-lined autoclave at 180°C for 12 h. The urea decomposed to release gases, which expanded the GO into a porous hydrogel, and at the same time, nitrogen was doped into the graphene matrix. The hydrogel was freeze-dried to maintain its three-dimensional structure. XPS complemented the incorporation of pyridinic, pyrrolic, and graphitic nitrogen into the carbon lattice. The N-GA reached 356 F/g at 1 A/g and had an energy density of 17.8 Wh/kg. Although possessing high electrochemical performance and high cycling stability (retention of 93.5% after 10,000 cycles), the batch nature of hydrothermal synthesis, in combination with the high cost and time-consuming nature of freeze-drying, limits scalability [161]. At an industrial scale, it is also challenging to control uniform foaming.

A different synthetic strategy involves the combination of chemical reduction plus freeze-casting, or 'freeze-thaw' processing, to eliminate the need for autoclaves. A recently reported co-doped aerogel with a mixture of ammonium sulfate (for S) and EDA (for N) was added to GO; hydrothermal gelation followed by a simple freeze-thaw cycle and ambient-pressure drying yielded an SN-GA [140, 162]. The SN-GA2 sample showed similar values of 244 F/g at 1 A/g and 18.1 Wh/kg at ~498 W/kg, as many of the freeze-dried GAs [140]. Importantly, this ambient-pressure drying method bypasses the use of costly freeze-dryers or supercritical CO_2 drying, thus enhancing scalability. Nonetheless, straightforward dehydrations may well involve the physisorption of some chemicals, and increasing the open porosity of the material commonly requires using additional methods such as hydrophobic agents and structural templates. Although the freeze-thaw was achievable in the SN-GA work because the polymeric soft segments (PDA and PANI) effectively 'locked in' the network, such multi-component gels can be expensive and non-homogeneous. Conversely, GO/N mixtures have been demonstrated to be 3D printable. For instance, one recent work in 2022 used direct-ink-writing to print a lattice of GO ink, which was plasma-treated to provide N_{12} a space where the resultant 3D-printed N-GA was utilised as a host for a sodium-metal battery, displaying a high efficiency but without supercapacitor data, which also indicates that additive manufacturing can yield customised electrode shapes [163]. Overall, printing or coating techniques provide high-structure fidelity but are still low-throughput and highly reliant on precise ink formulation. In general, the key takeaway is that those methods of assembly that do not require high temperatures (such as freeze-thaw or 3D ink writing) will generally be able to bypass the need for large autoclaves but will still necessitate continuous processing technologies, which remain in the first phases of research and development.

A separate branch of approaches uses templates or scaffolds at the time of GA formation. Some studies have incorporated sacrificial templates (salt crystals, polymer beads) with GO and N precursors for the generation of templated porosity. An important and broad example is the salt-templated chemical vapour deposition technique (CVD) [164, 165], in which N-doped graphene sheets are formed from exposing carbon precursors to ammonia gas under the guidance of molten salt matrices. These CVD processes can supply quantities of N-doped graphene in bulk and can be replicated to generate 3D salt-templated frameworks. Even so, the products made are typically either powders or films rather than freestanding aerogels. Other templating alternatives include metal-organic frameworks (MOFs) or ice. An example can be seen with the CVD approach, which focused on the creation of N-doped porous graphene, which used a mixture of melamine and Ni nanoparticles, which would be the template. The process is said to have achieved a highly functionalised graphene hybrid architecture that has a substantial pyridinic configuration with doping levels of nitrogen being as high as 12.7 at.% [164]. In another method, methane and pyridine were used, and this led to a high surface area of 1531 m^2/g. These methods are limited in scale due to the high cost of the MOF precursors and because they require being etched out of the templates. However, MOF-carbonisation methods are regarded as attractive approaches to simultaneously tailor pore structure and introduce a high heteroatom content in a one-pot process.

NGAs were also prepared through the process of sol-gel polymerisation, and then they would undergo freeze-drying and a high-temperature pyrolysis process in another study. It involves the formation of a resorcinol–formaldehyde (RF) gel matrix using resorcinol and formaldehyde as the main carbon sources, which is the first step of the process. Melamine was used as the nitrogen-containing precursor and was important to obtain nitrogen doping in the aerogel structure. A cross-linked hydrogel network was generated in a sol-gel paired regime and aged for structural stability. Afterwards, it was freeze-dried to eliminate water but maintain its highly porous three-dimensional structure. This is an important step to keep the surface area and pore connection needed for electrochemical applications. Following drying, the material was subjected to pyrolysis in an inert nitrogen atmosphere (usually near 800°C), during which melamine decomposed, releasing nitrogen species that chemically bond to the carbon framework, creating nitrogen functionalities (graphitic-N, pyridinic-N, and pyrrolic-N). Based on this study, the nitrogen-doped graphene aerogel exhibited a specific capacitance of 245 F/g at 1 A/g of current density, and the material exhibited stable cycling inhibition,

which confirms its utility for supercapacitor applications. These structural features, like high surface area with interconnected pores, enabled fast ion transport and charge storage. The sol-gel process is dependent on stoichiometric ratios and reaction conditions, which must be carefully controlled in order to produce high-quality graphene-based aerogels [166]. Plus, freeze-drying is energy- and time-intensive and thus impractical for industrial-scale production. Pyrolysis requires a high thermal input and operating in an inert environment, which makes its industrial implementation even more difficult. Therefore, although this approach offers superior structural and electrochemical properties, it requires some development towards an economically advantageous and highly scalable mass production.

From this, it is quite clear that hydrothermal reduction is one of the most widely accepted and adopted strategies that are used for synthesising various types of graphene aerogels; while other techniques have shown promising improvements, they are not yet as effective or usable as hydrothermal reduction, which makes them the primary choice. Table 5 provides a comparison of the various synthesis methods used for GAs.

7 | Discussion

The growing need for energy storage systems with effective and sustainable storage mechanisms makes GAs the perfect material for high-performance supercapacitor electrodes; this is because they have a high surface area, porosity, and 3D network, which tackle the common problems like stacking and poor ion movement seen in graphene-based materials. Of all the diverse modifications that are made to improve their electrochemical behaviour and overcome their limitations, nitrogen doping has been one of the most extraordinary strategies developed. By examining the synthesis techniques used, the impact of nitrogen on the internal structure, the potential for large-scale production, and the effectiveness of N-doped graphene aerogels as supercapacitor electrodes, the article concentrated on the most recent research conducted on NGAs over the previous 5 years. The results would support the study goal, which is that nitrogen doping, doping level, and synthesis technique are all important factors in optimising NGA frameworks.

The choice and design of the synthesis method are among the most important factors affecting the performance of NGAs. Various synthesis strategies have been explored in this article, such as hydrothermal reduction, sol-gel polymerisation, freeze-drying, pyrolysis, dual-template strategies, and CVD. For instance, the use of urea or melamine as nitrogen precursors, along with a one-step hydrothermal self-assembly method, enables simultaneous foaming and doping. This method is characterised by straightforwardness, low cost, and the ability to obtain aerogels with high specific capacitance (430 F/g) and high energy density (17.8 Wh/kg). Nevertheless, the batch nature of the process and the limitations of freeze-drying are the main factors leading to limited industrial scalability. However, these methods are good at entrapping pyridinic and graphitic nitrogen groups, which improve the conductivity and faradaic reactions. Likewise, dual-template-assisted approaches based on, for example, polystyrene beads and melamine enable a hierarchical pore structure. The generation of macro- and mesopores, moreover, enhances ion diffusion kinetics, which leads to aerogels with favourable ion diffusion properties. High performance has been demonstrated with specific capacitance values of ~402 F/g and energy densities of ~28 Wh/kg. However, these strategies bring extra environmental and economic stipulations, especially due to the subtraction of sacrificial templates and the crucial demand for exact regulation of the pore structure. Yet, they provide a useful strategy to design aerogels with desired performance through their structure.

In addition, sol-gel polymerisation involving both freeze-drying and pyrolysis is another strong synthetic route, reflected in studies of resorcinol–formaldehyde frameworks doped with melamine. They feature homogeneous nitrogen distribution, a high specific capacitance (245 F/g), and excellent cycle stability. Melamine is a substance that raises nitrogen levels while still providing structural integrity. Once again, the main drawbacks are the precursor batch sensitivity of the sol-gel system and the energy requirements linked to freeze-drying and pyrolysis. Such challenges are representative of most lab-scale syntheses and point to a fundamental trade-off between microstructural precision and scalability. Structurally, the configuration of nitrogen inside the carbon matrix is known to influence the electrochemical performance and behaviour of the final NGA. Among the various N species, pyridinic-N and graphitic-N are especially important because they not only promote electrical conductivity but also supply more active sites for pseudocapacitance. The utilisation of urea, EDA, and melamine tends to enhance the fraction of these nitrogen types, particularly after being carbonised at 800°C, and the resultant three-dimensional porous structure, obtained through freeze-drying and self-assembly, makes it easier for electrolyte access while reducing ion diffusion resistance, enabling high power densities and rate performance.

NS–rGOA is one of the most promising candidates due to the fact that the specific capacitance and other electrochemical properties of the material are found to be as high as 931 F/g, 36.56 Wh/kg, and 96% cyclic stability after 10,000 cycles, respectively. These outcomes constitute the best balance of optimal charge storage with continual carbon fibre structural durability in both two- and three-electrode configurations. This high performance stems from well-optimised internal porous properties and efficient nitrogen doping, which is probably composed of pyridinic and graphitic nitrogen species, resulting in high conductivity and pseudocapacitance. The retained high specific capacitance values of NG/MnO_2 and Co_3O_4-ZnO/NGA (609.9 F/g and 543 F/g, respectively) also accompany the good cycle life (up to 98% retention reported for NG/MnO_2). Moreover, it seems that metal oxide plays a helpful role in increasing the faradaic contribution and making ion accessibility more efficient. However, it is unclear whether these composites would be suitable for a device that requires a sustained energy output over time, since no energy densities have been reported. On the other hand, NGA (Asn) exceeds 80,000 cycles at a retention rate of 99.3%—a value that rarely occurs among any porous carbon-based supercapacitors. Although it has moderate specific capacitance (291.6 F/g) and a high energy density (23.8 Wh/kg), its performance and extreme durability will make it ideal for long-term commercial applications, especially in extreme or repeat charge-discharge situations.

TABLE 5 | Synthesis methods comparison.

Method	Main disadvantages	Scalability	Cost	Environmental impact	Remarks	Source
Hydrothermal	Requires high temperature/pressure and long reaction times; limited control over pore uniformity; high energy consumption.	Moderate	Moderate	Moderate	Typically followed by freeze- or supercritical drying; produces moderate-strength aerogel (~0.2–0.8 MPa); dopants introduced via solution precursors.	[167]
Sol–gel	Requires organic crosslinkers/ polymerization steps; often needs high-temperature curing or pyrolysis.	Moderate	Moderate	Moderate	Involves GO with resins (e.g. resorcinol–formaldehyde) and gelation; after drying and carbonization gives high-surface-area carbon aerogel.	[167]
Freeze drying	Slow, batch-wise process; high energy consumption due to the low-pressure freezing.	Moderate	High	Moderate	Common drying step for GO hydrogels; yields very high porosity; scalable (large freeze dryers); often used after hydrothermal, chemical reduction or sol–gel synthesis.	[167]
Supercritical drying	Requires high-pressure CO_2 equipment; expensive setup and operational costs.	Low	High	Moderate	Avoids capillary forces during drying; used when maximum surface area is needed; yields very low shrinkage, but limited throughput.	[167]
CVD	Requires sophisticated vacuum/high-temperature equipment; typically yields 2D films (needs template for 3D); low throughput and high energy use; hazardous gases may be required.	Low	High	Moderate–High	Grows graphene on substrates or foams (e.g. Ni foam); doping by NH_3, B_2H_6, PH_3, CF_4 gases; often multi-step (CVD + etching) to get freestanding aerogel.	[111]
Solvothermal	Involves flammable or toxic solvents (costly, safety issues); specialized equipment still needed; may require post-treatment.	Moderate	Moderate	Moderate–High	Uses organic solvents (e.g., DMSO, DMF) as reaction medium; single-source precursors (like thioethers) allow direct S- or N-doping; high surface area products.	[168]
Plasma treatment	Surface-only modification (limited depth); requires vacuum/plasma system; plasma parameters critically affect results.	Low	High	Low	Commonly used for N-doping with NH_3 plasma or for reduction in Ar/H_2; can restore sp^2 carbon; no additional chemicals needed.	[169]
3D printing	Requires carefully formulated GO inks (rheology) and post-processing; limited resolution (layer thickness); slower printing throughput.	Moderate	Moderate–High	Moderate	Direct ink writing of GO or GO/composite inks, followed by freeze- or supercritical drying; enables engineered lattices with high elasticity and fatigue resistance.	[167]

That said, there are some materials that disappoint compared to their counterparts. One of the best examples of this would be N/S-GA-2, and from the findings, it is quite clear that it has a low specific capacitance value, which is not as high as the other models at 169.4 F/g, and the poorest cycle life in comparison to the other studies, with 3000 cycles in which it retains only 77.2%. This may be due to insufficient nitrogen doping and/or the unstable electrode-electrolyte interface. Moreover, NCA from APMP is also one of the least favourable entries, with only 185 F/g of capacitance and no data on cycling stability and energy density available. This lack of such critical parameters in many studies limits their relevance in comparative studies and highlights the need for systematic and standardised characterisation. However, while several materials show individual merits, the data set highlights a pervasive inconsistency of reported values, hindering comprehensive performance benchmarking. Though many studies present extensive data on specific capacitance and cycling stability, often reporting thousands to tens of thousands of cycles, energy density, a critical performance parameter for practical applicability, is rarely included. Consistently, materials like Co_3O_4-ZnO/NGA, NG/MnO_2, and BN-HGA achieve remarkable capacitance and cycling properties while omitting any relevant energy density information, making it hard to determine the complete storage capability. In contrast, while NPHG and DHAQ-NGA show high energy density capacities, there is an ambiguity regarding long-term degradation or possible operational voltage windows. Such inconsistency further emphasises the necessity for standardised and comprehensive reporting, namely with respect to energy and power density values obtained using two-electrode set-ups, which more closely mimic realistic device operation. It is only by such uniform benchmarking that materials can be compared in a meaningful way, and steps toward commercialisation at scale can be taken.

Going forward, the focus of research should be the scale-up of the synthesis methods while maintaining performance. Common practices such as freeze-drying, hydrothermal reduction process, and post-carbonisation treatments are energy-consumptive and batch-limited. This prompts the immediate need for investigation of alternative synthesis strategies. For instance, microwave-assisted hydrothermal synthesis shortens processing time and can also aid in uniform doping. Similarly, aerosol-assisted self-assembly towards scalable template-free fabrication of porous structures. In addition, electrochemical doping and self-healing methods introduce nitrogen functionalities post-aerogel formation without aggressive heat treatments. Moreover, scalable fabrication techniques such as spray drying and inkjet printing would allow for commercial-scale production of flexible, device-ready electrodes.

More importantly, research on heteroatom co-doping, such as nitrogen-sulfur, nitrogen-boron, and nitrogen-phosphorus systems, needs to go much deeper to illustrate the combination effect for additional improvement of electrochemical behaviours. Although a few dual-doped systems have been utilised (e.g., N/S-GA-2, SNGA4-BII), their combination of multiple dopant species and the interaction of dopants have not been well characterised with regard to structure-property relationships. Lastly, there is a greater need to focus on studying long-term degradation mechanisms, especially under the conditions of use (e.g., high temperature, mechanical flexing (for flexible/wearable devices), or non-aqueous electrolytes). Notably, materials such as BN-HGA that have been tested in flexible configurations pave the way toward these applications, but robust assessments of stability under a dynamic environment are largely absent. Also, a lack of thorough research on controlling porosity and pore size is observed in the existing literature, given that these two factors are major for charge storage. Even though some works categorize materials as either mesoporous or microporous, few provide a sure method for managing the mix of different pore sizes. It is crucial that pore diameters are precisely aligned with the size of electrolyte ions, including their solvation shells, for EDL capacitance and ion transport efficiency. A number of studies indicate that discrepancies between pore size and ion size can substantially impede ion accessibility, diminish charge storage, and decrease rate capacity. Consequently, standardising the reporting and discourse on pore structure regulation, while explicitly accounting for electrolyte ion dimensions, would significantly expedite the advancement of next-generation supercapacitors, potentially achieving performance metrics that match or exceed those of batteries.

Overall, while some NGA systems currently provide impressive performance in certain categories, the wider field now needs to focus on balancing electrochemical performance with manufacturability. The study proposes that future work is directed towards more sustainable and scalable synthesis routes, standardisation of test conditions and improved reporting of detailed electrochemical profiles to allow for rational comparisons and fast-tracked commercial translation.

8 | Conclusion

Graphene aerogels containing nitrogen have emerged as a competitive material class for the cutting-edge supercapacitor electrode. Furthermore, carbon materials' unique three-dimensional porous structure, high electrical conductivity, and adjustable surface chemistry make them perfect for long-term cycle stability, high capacitance, and high charge-discharge rates. Recent research has demonstrated that even trace levels of nitrogen doping significantly alter structural and electrochemical characteristics. In addition to producing pseudocapacitive sites, the nitrogen atoms also adjust the material's electronic structure, increasing surface polarity and electrical conductivity. Large specific capacitance (> 900 F/g), large energy densities, and exceptional stability (up to thousands of cycles) were attained by the best examples, such as NS–rGOA3, NHGA, and NG/MnO_2-400. N-GA-4 (Asn), for example, which retains 99.3% after 80,000 cycles; such durability can be obtained through well-designed aerogel architecture and optimised doping. The above successes are also a reminder of the potential for nitrogen doping with other burying materials, for instance, metal oxides or conductive polymers, which can have a synergistic effect.

However, a large gulf remains between success at the laboratory and industrial scale-up. A number of the synthesis methods—like hydrothermal assembly, freeze-drying, and high-temperature pyrolysis—are still impractical for the switch to mass production. These processes typically demand long processing times, high energy inputs, and stringent control over operating conditions, which restricts batch reproducibility and economic viability. Also, with fewer related routes, it uses toxic chemicals or generates lots of waste, which counteract some of the aims of sustainable energy storage solutions. A constant problem has been the lack of

consistency in testing protocols and how performance is reported. Some studies report full electrochemical characterisation, while others simply do not include key data (e.g., energy density or cycle life). In addition, most reports use three-electrode configurations, which lead to performance overestimations for real two-electrode devices. For accurate benchmarking and comparison of materials, further studies should utilise standardised procedures, including performance testing in a relevant device setting.

Going forward, the focus should be on synthesis methods that are scalable and sustainable. Fabrication methods like microwave-assisted synthesis, spray-drying, sol-gel templating, and direct ink writing could pave the way towards morphology- and dopant-composition controllable mass-producible aerogels. These approaches are capable of decreasing energy consumption, minimising the number of process steps, and allowing for continuous or semi-continuous fabrication. Simultaneously, further attention to the heteroatom co-doping with sulfur, boron, or phosphorus, in addition to nitrogen, could increase the redox activity, surface wettability, and ion diffusion kinetics.

While beyond the scope of this work, future development of NGAs will also need to address integration into flexible and hybrid energy storage platforms in tandem, using common parameterisation for performance and scalability. Although many studies have indicated the possibility of a wearable form of supercapacitors and solid-state configuration, these two important areas have not yet been widely explored as required, and some of the reviewed materials have shown high flexibility, making the materials more attractive as a future solution. Lastly, more mechanistic studies relating nitrogen configuration (e.g., pyridinic, pyrrolic, and graphitic) to electrochemical performance are needed to allow the design of the next generation of aerogels. Nitrogen-doped graphene aerogels are promising candidates for high-performance, long-cycle-life, and potentially high-throughput supercapacitor materials.

Acknowledgments

The authors would like to acknowledge the financial support from Universiti Teknologi Malaysia under UTM Flagship CoE/RG Research Grants (Q.J130000.5009.10G17 and Q.J130000.5023.10G18).

Conflicts of Interest

The authors declare no conflicts of interest.

References

1. Y. Tingting, L. Ruiyi, L. Xiaohuan, et al., "Nitrogen and Sulphur-Functionalized Multiple Graphene Aerogel for Supercapacitors With Excellent Electrochemical Performance," *Electrochimica Acta* 187 (2016): 143–152, https://doi.org/10.1016/j.electacta.2015.11.043.

2. X. Cui, S. Yang, X. Yan, et al., "Pyridinic-Nitrogen-Dominated Graphene Aerogels With Fe–N–C Coordination for Highly Efficient Oxygen Reduction Reaction," *Advanced Functional Materials* 26 (2016): 5708–5717, https://doi.org/10.1002/adfm.201601492.

3. K. A. A. A. Elsehsah, Z. Ahmad Noorden, and N. Mat Saman, "Current Insights and Future Prospects of Graphene Aerogel-Enhanced Supercapacitors: A Systematic Review," *Heliyon* 10 (2024): e37071, https://doi.org/10.1016/j.heliyon.2024.e37071.

4. C. Bacon, A. Serva, C. Merlet, P. Simon, and M. Salanne, "On the Key Role of Electrolyte–Electrode Van Der Waals Interactions in the Simulation of Ionic Liquids-Based Supercapacitors," *Electrochimica Acta* 455 (2023): 142380, https://doi.org/10.1016/j.electacta.2023.142380.

5. D. P. Chatterjee and A. K. Nandi, "A Review on the Recent Advances in Hybrid Supercapacitors," *Journal of Materials Chemistry A* 9 (2021): 15880–15918, https://doi.org/10.1039/D1TA02505H.

6. W. Yang, J. Tan, J. Wang, et al., "Enhancing Mechanical and Flame Retardant Properties of Carbon Fibre Epoxy Composites With Functionalised Ammonium Polyphosphate Nanoparticles," *Composites Science and Technology* 261 (2025): 111005, https://doi.org/10.1016/j.compscitech.2024.111005.

7. Z. Ayaganov, V. Pavlenko, S. F. B. Haque, et al., "A Comprehensive Study on Effect of Carbon Nanomaterials as Conductive Additives in EDLCs," *Journal of Energy Storage* 78 (2024): 110035, https://doi.org/10.1016/j.est.2023.110035.

8. D. Bejjanki and S. K. Puttapati, "Supercapacitor Basics (EDLCs, Pseudo, and Hybrid)," in *Multidimensional Nanomaterials for Supercapacitors: Next Generation Energy Storage* (Bentham Science Publishers, 2024), 29–48, https://www.benthamdirect.com/content/books/9789815223408.chapter-2.

9. Z. Cheng, R. Wang, Y. Wang, et al., "Recent Advances in Graphene Aerogels as Absorption-Dominated Electromagnetic Interference Shielding Materials," *Carbon* 205 (2023): 112–137, https://doi.org/10.1016/j.carbon.2023.01.032.

10. G. Gorgolis and C. Galiotis, "Graphene Aerogels: A Review," *2D Materials* 4 (2017): 032001, https://doi.org/10.1088/2053-1583/aa7883.

11. S. Korkmaz and İ. A. Kariper, "Graphene and Graphene Oxide Based Aerogels: Synthesis, Characteristics and Supercapacitor Applications," *Journal of Energy Storage* 27 (2020): 101038, https://doi.org/10.1016/j.est.2019.101038.

12. M. S. Çögenli and A. Bayrakçeken Yurtcan, "Heteroatom Doped 3D Graphene Aerogel Supported Catalysts for Formic Acid and Methanol Oxidation," *International Journal of Hydrogen Energy* 45 (2020): 650–666, https://doi.org/10.1016/j.ijhydene.2019.10.226.

13. N. Fernández-Sáez, D. E. Villela-Martinez, F. Carrasco-Marín, A. F. Pérez-Cadenas, and L. M. Pastrana-Martínez, "Heteroatom-Doped Graphene Aerogels and Carbon-Magnetite Catalysts for the Heterogeneous Electro-Fenton Degradation of Acetaminophen in Aqueous Solution," *Journal of Catalysis* 378 (2019): 68–79, https://doi.org/10.1016/j.jcat.2019.08.020.

14. Z.-Y. Sui, Y.-N. Meng, P.-W. Xiao, Z.-Q. Zhao, Z.-X. Wei, and B.-H. Han, "Nitrogen-Doped Graphene Aerogels as Efficient Supercapacitor Electrodes and Gas Adsorbents," *ACS Applied Materials & Interfaces* 7 (2015): 1431–1438, https://doi.org/10.1021/am5042065.

15. M. El-Kady, "Graphene Supercapacitors: Charging Up the Future" (Doctoral, University of California, 2013).

16. R. K. Singh, S. K. Mishra, and V. V. Mehtre, "Supercapacitor Construction, Principle, Operation, Characteristics, Advantages, Disadvantages and Applications," *International Journal of Innovative Research in Electrical, Electronics, Instrumentation and Control Engineering* 9 (2021): 189–194.

17. S. Sharma and P. Chand, "Supercapacitor and Electrochemical Techniques: A Brief Review," *Results in Chemistry* 5 (2023): 100885, https://doi.org/10.1016/j.rechem.2023.100885.

18. Y. Guan, K. Hu, N. Su, G. Zhang, Y. Han, and M. An, "Review of NiS-Based Electrode Nanomaterials for Supercapacitors," *Nanomaterials* 13 (2023): 979, https://doi.org/10.3390/nano13060979.

19. M. Şahin, F. Blaabjerg, and A. Sangwongwanich, "A Comprehensive Review on Supercapacitor Applications and Developments," *Energies* 15 (2022): 674, https://doi.org/10.3390/en15030674.

20. Z. Végvári, "Supercapacitors and Their Military Applicability," *Honvédségi Szemle—Hungarian Defence Review* 147 (2019): 38–49, https://doi.org/10.35926/HDR.2019.1-2.3.

21. D. O. Reid, "Advanced Fibre Based Energy Storage" (Doctoral thesis, University of Surrey, 2016).

22. P. Forouzandeh, V. Kumaravel, and S. C. Pillai, "Electrode Materials for Supercapacitors: A Review of Recent Advances," *Catalysts* 10 (2020): 969, https://doi.org/10.3390/catal10090969.

23. A. Velasco, Y. K. Ryu, A. Boscá, et al., "Recent Trends in Graphene Supercapacitors: From Large Area to Microsupercapacitors," *Sustainable Energy & Fuels* 5 (2021): 1235–1254, https://doi.org/10.1039/D0SE01849J.

24. J. Zhao and A. F. Burke, "Review on Supercapacitors: Technologies and Performance Evaluation," *Journal of Energy Chemistry* 59 (2021): 276–291, https://doi.org/10.1016/j.jechem.2020.11.013.

25. K. Kraiwattanawong, "A Review on the Development of a Porous Carbon-Based as Modeling Materials for Electric Double Layer Capacitors," *Arabian Journal of Chemistry* 15 (2022): 103625, https://doi.org/10.1016/j.arabjc.2021.103625.

26. X. Chen, L. Qiu, J. Ren, et al., "Novel Electric Double-Layer Capacitor With a Coaxial Fiber Structure," *Advanced Materials* 25 (2013): 6436–6441, https://doi.org/10.1002/adma.201301519.

27. C. Largeot, C. Portet, J. Chmiola, P.-L. Taberna, Y. Gogotsi, and P. Simon, "Relation Between the Ion Size and Pore Size for an Electric Double-Layer Capacitor," *Journal of the American Chemical Society* 130 (2008): 2730–2731, https://doi.org/10.1021/ja7106178.

28. R. Burt, G. Birkett, and X. S. Zhao, "A Review of Molecular Modelling of Electric Double Layer Capacitors," *Physical Chemistry Chemical Physics* 16 (2014): 6519–6538, https://doi.org/10.1039/C3CP55186E.

29. K. Liang, R. A. Matsumoto, W. Zhao, et al., "Engineering the Interlayer Spacing by Pre-Intercalation for High Performance Supercapacitor MXene Electrodes in Room Temperature Ionic Liquid," *Advanced Functional Materials* 31 (2021): 2104007, https://doi.org/10.1002/adfm.202104007.

30. N. C. Osti and E. Mamontov, "Microscopic Dynamics in Room-Temperature Ionic Liquids Confined in Materials for Supercapacitor Applications," *Sustainable Energy & Fuels* 4 (2020): 1554–1576, https://doi.org/10.1039/C9SE00829B.

31. P. Pietrzyk-Thel, A. Jain, K. Bochenek, et al., "Flexible, Tough and High-Performing Ionogels for Supercapacitor Application," *Journal of Materiomics* 11 (2025): 100833, https://doi.org/10.1016/j.jmat.2024.01.008.

32. V. D. Ivanov, "The Helmholtz Model," *Journal of Solid State Electrochemistry* 28 (2024): 2487–2493, https://doi.org/10.1007/s10008-024-05850-5.

33. G. C. Gschwend, A. Olaya, and H. H. Girault, "How to Polarise an Interface With Ions: The Discrete Helmholtz Model," *Chemical Science* 11 (2020): 10807–10813, https://doi.org/10.1039/D0SC00685H.

34. K. Masuyama, "Electrochemistry of Room Temperature Ionic Liquids With Applications to Electrospray Propulsion" (Doctoral thesis, Massachusetts Institute of Technology, 2016).

35. G. Srividhya and N. Ponpandian, "Pseudocapacitance: Mechanism and Characteristics," in *Pseudocapacitors: Fundamentals to High Performance Energy Storage Devices*, ed. R. K. Gupta (Springer Nature Switzerland, 2024), 39–56, https://doi.org/10.1007/978-3-031-45430-1_3.

36. P. M. Biesheuvel and A. van der Wal, "Membrane Capacitive Deionization," *Journal of Membrane Science* 346 (2010): 256–262, https://doi.org/10.1016/j.memsci.2009.09.043.

37. X. Liu, C. Shi, C. Zhai, M. Cheng, Q. Liu, and G. Wang, "Cobalt-Based Layered Metal–Organic Framework as an Ultrahigh Capacity Supercapacitor Electrode Material," *ACS Applied Materials & Interfaces* 8 (2016): 4585–4591, https://doi.org/10.1021/acsami.5b10781.

38. R. Ramachandran, C. Zhao, D. Luo, K. Wang, and F. Wang, "Morphology-Dependent Electrochemical Properties of Cobalt-Based Metal Organic Frameworks for Supercapacitor Electrode Materials," *Electrochimica Acta* 267 (2018): 170–180, https://doi.org/10.1016/j.electacta.2018.02.074.

39. A. Yu, V. Chabot, and J. Zhang, *Electrochemical Supercapacitors for Energy Storage and Delivery: Fundamentals and Applications* (CRC Press, 2017), https://doi.org/10.1201/b14671.

40. C. T. Tshiani and P. Umenne, "The Impact of the Electric Double-Layer Capacitor (EDLC) in Reducing Stress and Improving Battery Lifespan in a Hybrid Energy Storage System (HESS) System," *Energies* 15 (2022): 8680, https://doi.org/10.3390/en15228680.

41. V. V. Jadhav, R. S. Mane, and P. V. Shinde, "Electrochemical Supercapacitors: History, Types, Designing Processes, Operation Mechanisms, and Advantages and Disadvantages," in *Bismuth-Ferrite-Based Electrochemical Supercapacitors*, eds. V. V. Jadhav, R. S. Mane, and P. V. Shinde (Springer International Publishing, 2020), 11–36, https://doi.org/10.1007/978-3-030-16718-9_2.

42. D. Tashima, A. K. Samantara, T. Prasankumar, J. Jose, S. Jose, and S. P. Balakrishnan, "Supercapacitors for the Next Generation," *Supercapacitors for the Next Generation* (IntechOpen, 2022), https://doi.org/10.5772/intechopen.94792.

43. P. Tang, W. Tan, G. Deng, et al., "Understanding Pseudocapacitance Mechanisms by Synchrotron X-Ray Analytical Techniques," *Energy & Environmental Materials* 6 (2023): e12619, https://doi.org/10.1002/eem2.12619.

44. X. Wu, H. Yang, M. Yu, J. Liu, and S. Li, "Design Principles of High-Voltage Aqueous Supercapacitors," *Materials Today Energy* 21 (2021): 100739, https://doi.org/10.1016/j.mtener.2021.100739.

45. N. R. Chodankar, H. D. Pham, A. K. Nanjundan, et al., "True Meaning of Pseudocapacitors and Their Performance Metrics: Asymmetric Versus Hybrid Supercapacitors," *Small* 16 (2020): 2002806, https://doi.org/10.1002/smll.202002806.

46. L. Cao, J. Zhu, Y. Li, et al., "Ultrathin Single-Crystalline Vanadium Pentoxide Nanoribbon Constructed 3D Networks for Superior Energy Storage," *Journal of Materials Chemistry A: Materials for Energy and Sustainability* 2 (2014): 13136–13142, https://doi.org/10.1039/C4TA02229G.

47. Z. Lu, R. Raad, F. Safaei, J. Xi, Z. Liu, and J. Foroughi, "Carbon Nanotube Based Fiber Supercapacitor as Wearable Energy Storage," *Frontiers in Materials* 6 (2019): 138, https://doi.org/10.3389/fmats.2019.00138.

48. A. Muzaffar, M. B. Ahamed, K. Deshmukh, and J. Thirumalai, "A Review on Recent Advances in Hybrid Supercapacitors: Design, Fabrication and Applications," *Renewable and Sustainable Energy Reviews* 101 (2019): 123–145, https://doi.org/10.1016/j.rser.2018.10.026.

49. D. Gao, Z. Luo, C. Liu, and S. Fan, "A Survey of Hybrid Energy Devices Based on Supercapacitors," *Green Energy & Environment* 8 (2023): 972–988, https://doi.org/10.1016/j.gee.2022.02.002.

50. V. Khomenko, E. Raymundo-Piñero, and F. Béguin, "High-Energy Density Graphite/AC Capacitor in Organic Electrolyte," *Journal of Power Sources* 177 (2008): 643–651, https://doi.org/10.1016/j.jpowsour.2007.11.101.

51. G. G. Amatucci, F. Badway, A. Du Pasquier, and T. Zheng, "An Asymmetric Hybrid Nonaqueous Energy Storage Cell," *Journal of the Electrochemical Society* 148 (2001): A930, https://doi.org/10.1149/1.1383553.

52. D. Cericola and R. Kötz, "Hybridization of Rechargeable Batteries and Electrochemical Capacitors: Principles and Limits," *Electrochimica Acta* 72 (2012): 1–17, https://doi.org/10.1016/j.electacta.2012.03.151.

53. M. Mounika, G. Dilip Kumar, and D. Danalakshmi, "Evolution of Hybrid Super Capacitors and Its Future Pathway," *International Journal of Engineering Applied Sciences and Technology* 4 (2019): 114–119.

54. K. Naoi, S. Ishimoto, J. Miyamoto, and W. Naoi, "Second Generation 'Nanohybrid Supercapacitor': Evolution of Capacitive Energy Storage

Devices," *Energy & Environmental Science* 5 (2012): 9363–9373, https://doi.org/10.1039/C2EE21675B.

55. K. Naoi, "Nanohybrid Capacitor': The Next Generation Electrochemical Capacitors," *Fuel Cells* 10 (2010): 825–833, https://doi.org/10.1002/fuce.201000041.

56. C. Merlet, B. Rotenberg, P. A. Madden, et al., "On the Molecular Origin of Supercapacitance in Nanoporous Carbon Electrodes," *Nature Materials* 11 (2012): 306–310, https://doi.org/10.1038/nmat3260.

57. P. Simon and Y. Gogotsi, "Materials for Electrochemical Capacitors," *Nature Materials* 7 (2008): 845–854, https://doi.org/10.1038/nmat2297.

58. T. Prasankumar, J. Jose, S. Jose, and S. P. Balakrishnan, "Pseudocapacitors," *Supercapacitors for the Next Generation* (IntechOpen, 2022), https://doi.org/10.5772/intechopen.98600.

59. V. Augustyn, J. Come, M. A. Lowe, et al., "High-Rate Electrochemical Energy Storage Through Li^+ Intercalation Pseudocapacitance," *Nature Materials* 12 (2013): 518–522, https://doi.org/10.1038/nmat3601.

60. X. Yu, S. Yun, J. S. Yeon, et al., "Emergent Pseudocapacitance of 2D Nanomaterials," *Advanced Energy Materials* 8 (2018): 1702930, https://doi.org/10.1002/aenm.201702930.

61. C. Choi, D. S. Ashby, D. M. Butts, et al., "Achieving High Energy Density and High Power Density With Pseudocapacitive Materials," *Nature Reviews Materials* 5 (2020): 5–19, https://doi.org/10.1038/s41578-019-0142-z.

62. J. Zhang, A. Yu, and V. Chabot, *Electrochemical Supercapacitors for Energy Storage and Delivery Fundamentals and Applications* (Taylor & Francis Group, 2014).

63. F. Barzegar, D. Y. Momodu, O. O. Fashedemi, A. Bello, J. K. Dangbegnon, and N. Manyala, "Investigation of Different Aqueous Electrolytes on the Electrochemical Performance of Activated Carbon-Based Supercapacitors," *RSC Advances* 5 (2015): 107482–107487, https://doi.org/10.1039/c5ra21962k.

64. I. I. G. Inal and Z. Aktas, "Enhancing the Performance of Activated Carbon Based Scalable Supercapacitors by Heat Treatment," *Applied Surface Science* 514 (2020): 145895, https://doi.org/10.1016/j.apsusc.2020.145895.

65. T. Yumak, D. Bragg, and E. M. Sabolsky, "Effect of Synthesis Methods on the Surface and Electrochemical Characteristics of Metal Oxide/Activated Carbon Composites for Supercapacitor Applications," *Applied Surface Science* 469 (2019): 983–993, https://doi.org/10.1016/j.apsusc.2018.09.079.

66. M. I. A. A. Maksoud, R. A. Fahim, A. E. Shalan, et al., "Advanced Materials and Technologies for Supercapacitors Used in Energy Conversion and Storage: A Review," *Environmental Chemistry Letters* 19 (2021): 375–439, https://doi.org/10.1007/s10311-020-01075-w.

67. A. S. Lemine, M. M. Zagho, T. M. Altahtamouni, and N. Bensalah, "Graphene a Promising Electrode Material for Supercapacitors—A Review," *International Journal of Energy Research* 42 (2018): 4284–4300, https://doi.org/10.1002/er.4170.

68. H. P. Bei, Y. Yang, Q. Zhang, et al., "Graphene-Based Nanocomposites for Neural Tissue Engineering," *Molecules* 24 (2019): 658, https://doi.org/10.3390/molecules24040658.

69. Y. Ma, H. Chang, M. Zhang, and Y. Chen, "Graphene-Based Materials for Lithium-Ion Hybrid Supercapacitors," *Advanced Materials* 27 (2015): 5296–5308, https://doi.org/10.1002/adma.201501622.

70. M. D. Stoller, S. Murali, N. Quarles, et al., "Activated Graphene as a Cathode Material for Li-Ion Hybrid Supercapacitors," *Physical Chemistry Chemical Physics* 14 (2012): 3388, https://doi.org/10.1039/c2cp00017b.

71. R. Gokhale, V. Aravindan, P. Yadav, et al., "Oligomer-Salt Derived 3D, Heavily Nitrogen Doped, Porous Carbon for Li-Ion Hybrid Electrochemical Capacitors Application," *Carbon* 80 (2014): 462–471, https://doi.org/10.1016/j.carbon.2014.08.086.

72. V. Aravindan, D. Mhamane, W. C. Ling, S. Ogale, and S. Madhavi, "Nonaqueous Lithium-Ion Capacitors With High Energy Densities Using Trigol-Reduced Graphene Oxide Nanosheets as Cathode-Active Material," *Chemsuschem* 6 (2013): 2240–2244, https://doi.org/10.1002/cssc.201300465.

73. H. Wang, C. Guan, X. Wang, and H. J. Fan, "A High Energy and Power Li-Ion Capacitor Based on a TiO2 Nanobelt Array Anode and a Graphene Hydrogel Cathode," *Small* 11 (2015): 1470–1477, https://doi.org/10.1002/smll.201402620.

74. S.-M. Lee, J.-H. Kim, and J.-H. Ahn, "Graphene as a Flexible Electronic Material: Mechanical Limitations by Defect Formation and Efforts to Overcome," *Materials Today* 18 (2015): 336–344, https://doi.org/10.1016/j.mattod.2015.01.017.

75. L. Ye, Q. Liang, Y. Lei, et al., "A High Performance Li-Ion Capacitor Constructed With $Li_4Ti_5O_{12}$/C Hybrid and Porous Graphene Macroform," *Journal of Power Sources* 282 (2015): 174–178, https://doi.org/10.1016/j.jpowsour.2015.02.028.

76. D. Guo, S. Dou, X. Li, et al., "Hierarchical MnO2/rGO Hybrid Nanosheets as an Efficient Electrocatalyst for the Oxygen Reduction Reaction," *International Journal of Hydrogen Energy* 41 (2016): 5260–5268, https://doi.org/10.1016/j.ijhydene.2016.01.070.

77. J. J. Ren, L. W. Su, X. Qin, et al., "Pre-Lithiated Graphene Nanosheets as Negative Electrode Materials for Li-Ion Capacitors With High Power and Energy Density," *Journal of Power Sources* 264 (2014): 108–113, https://doi.org/10.1016/j.jpowsour.2014.04.076.

78. J. Jing, X. Qian, Y. Si, G. Liu, and C. Shi, "Recent Advances in the Synthesis and Application of Three-Dimensional Graphene-Based Aerogels," *Molecules* 27 (2022): 924, https://doi.org/10.3390/molecules27030924.

79. M. Kotal, J. Kim, J. Oh, and I. K. Oh, "Recent Progress in Multifunctional Graphene Aerogels," *Frontiers in Materials* 3 (2016): 29, https://doi.org/10.3389/fmats.2016.00029.

80. L. Qiu, R. Zhang, Y. Zhang, C. Li, Q. Zhang, and Y. Zhou, "Superhydrophobic, Mechanically Flexible and Recyclable Reduced Graphene Oxide Wrapped Sponge for Highly Efficient Oil/Water Separation," *Frontiers of Chemical Science and Engineering* 12 (2018): 390–399, https://doi.org/10.1007/s11705-018-1751-6.

81. H. Sun, Z. Xu, and C. Gao, "Multifunctional, Ultra-Flyweight, Synergistically Assembled Carbon Aerogels," *Advanced Materials (Deerfield Beach, Fla.)* 25 (2013): 2554–2560, https://doi.org/10.1002/adma.201204576.

82. M. A. Riaz, G. McKay, and J. Saleem, "3D Graphene-Based Nanostructured Materials as Sorbents for Cleaning Oil Spills and for the Removal of Dyes and Miscellaneous Pollutants Present in Water," *Environmental Science and Pollution Research* 24 (2017): 27731–27745, https://doi.org/10.1007/s11356-017-0606-x.

83. X. Zhang, J. Zhou, Y. Zheng, H. Wei, and Z. Su, "Graphene-Based Hybrid Aerogels for Energy and Environmental Applications," *Chemical Engineering Journal* 420 (2021): 129700, https://doi.org/10.1016/j.cej.2021.129700.

84. J. Mao, J. Iocozzia, J. Huang, K. Meng, Y. Lai, and Z. Lin, "Graphene Aerogels for Efficient Energy Storage and Conversion," *Energy & Environmental Science* 11 (2018): 772–799, https://doi.org/10.1039/C7EE03031B.

85. J. Liu, H. Qin, and Y. Liu, "Multi-Scale Structure-Mechanical Property Relations of Graphene-Based Layer Materials," *Materials* 14 (2021): 4757, https://doi.org/10.3390/ma14164757.

86. N. Ni, S. Barg, E. Garcia-Tunon, et al., "Understanding Mechanical Response of Elastomeric Graphene Networks," *Scientific Reports* 5 (2015): 13712, https://doi.org/10.1038/srep13712.

87. W. Gao, N. Zhao, W. Yao, Z. Xu, H. Bai, and C. Gao, "Effect of Flake Size on the Mechanical Properties of Graphene Aerogels Prepared by

Freeze Casting," *RSC Advances* 7 (2017): 33600–33605, https://doi.org/10.1039/c7ra05557a.

88. Y. Wu, N. Yi, L. Huang, et al., "Three-Dimensionally Bonded Spongy Graphene Material With Super Compressive Elasticity and Near-Zero Poisson's Ratio," *Nature Communications* 6 (2015): 7141, https://doi.org/10.1038/ncomms7141.

89. R. Ikram, B. M. Jan, and W. Ahmad, "An Overview of Industrial Scalable Production of Graphene Oxide and Analytical Approaches for Synthesis and Characterization," *Journal of Materials Research and Technology* 9 (2020): 11587–11610, https://doi.org/10.1016/j.jmrt.2020.08.050.

90. L. Qiu, B. Huang, Z. He, et al., "Extremely Low Density and Super-Compressible Graphene Cellular Materials," *Advanced Materials* 29 (2017): 1701553, https://doi.org/10.1002/adma.201701553.

91. L. dos Santos-Gómez, J. R. García, M. A. Montes-Morán, J. A. Menéndez, S. García-Granda, and A. Arenillas, "Ultralight-Weight Graphene Aerogels With Extremely High Electrical Conductivity," *Small* 17 (2021): 2103407, https://doi.org/10.1002/smll.202103407.

92. M. A. Worsley, P. J. Pauzauskie, T. Y. Olson, J. Biener, J. H. Satcher, and T. F. Baumann, "Synthesis of Graphene Aerogel With High Electrical Conductivity," *Journal of the American Chemical Society* 132 (2010): 14067–14069, https://doi.org/10.1021/ja1072299.

93. D. A. C. Brownson, D. K. Kampouris, and C. E. Banks, "An Overview of Graphene in Energy Production and Storage Applications," *Journal of Power Sources* 196 (2011): 4873–4885, https://doi.org/10.1016/j.jpowsour.2011.02.022.

94. F. Luan, G. Wang, Y. Ling, et al., "High Energy Density Asymmetric Supercapacitors With a Nickel Oxide Nanoflake Cathode and a 3D Reduced Graphene Oxide Anode," *Nanoscale* 5 (2013): 7984, https://doi.org/10.1039/c3nr02710d.

95. H. Gao, F. Xiao, C. B. Ching, and H. Duan, "High-Performance Asymmetric Supercapacitor Based on Graphene Hydrogel and Nanostructured MnO2," *ACS Applied Materials and Interfaces* 4 (2012): 2801–2810, https://doi.org/10.1021/am300455d.

96. S. M. Jung, D. L. Mafra, C. T. Lin, H. Y. Jung, and J. Kong, "Controlled Porous Structures of Graphene Aerogels and Their Effect on Supercapacitor Performance," *Nanoscale* 7 (2015): 4386–4393, https://doi.org/10.1039/c4nr07564a.

97. X. Wei, S. Wan, and S. Gao, "Self-Assembly-Template Engineering Nitrogen-Doped Carbon Aerogels for High-Rate Supercapacitors," *Nano Energy* 28 (2016): 206–215, https://doi.org/10.1016/j.nanoen.2016.08.023.

98. Z. Song, W. Liu, P. Xiao, Z. Zhao, G. Liu, and J. Qiu, "Nano-Iron Oxide (Fe_2O_3)/Three-Dimensional Graphene Aerogel Composite as Supercapacitor Electrode Materials With Extremely Wide Working Potential Window," *Materials Letters* 145 (2015): 44–47, https://doi.org/10.1016/j.matlet.2015.01.040.

99. T. T. Chen, W. L. Song, and L. Z. Fan, "Engineering Graphene Aerogels With Porous Carbon of Large Surface Area for Flexible All-Solid-State Supercapacitors," *Electrochimica Acta* 165 (2015): 92–97, https://doi.org/10.1016/j.electacta.2015.02.008.

100. Y. Liu, D. He, H. Wu, J. Duan, and Y. Zhang, "Hydrothermal Self-Assembly of Manganese Dioxide/Manganese Carbonate/Reduced Graphene Oxide Aerogel for Asymmetric Supercapacitors," *Electrochimica Acta* 164 (2015): 154–162, https://doi.org/10.1016/j.electacta.2015.01.223.

101. R. Kumar, S. Sahoo, E. Joanni, et al., "Heteroatom Doped Graphene Engineering for Energy Storage and Conversion," *Materials Today* 39 (2020): 47–65, https://doi.org/10.1016/j.mattod.2020.04.010.

102. X. Wang, G. Sun, P. Routh, D. H. Kim, W. Huang, and P. Chen, "Heteroatom-Doped Graphene Materials: Syntheses, Properties and Applications," *Chemical Society Reviews* 43 (2014): 7067–7098, https://doi.org/10.1039/c4cs00141a.

103. H. L. Guo, P. Su, X. Kang, and S. K. Ning, "Synthesis and Characterization of Nitrogen-Doped Graphene Hydrogels by Hydrothermal Route With Urea as Reducing-Doping Agents," *Journal of Materials Chemistry A* 1 (2013): 2248–2255, https://doi.org/10.1039/c2ta00887d.

104. Z. Zuo, Z. Jiang, and A. Manthiram, "Porous B-Doped Graphene Inspired by Fried-Ice for Supercapacitors and Metal-Free Catalysts," *Journal of Materials Chemistry A* 1 (2013): 13476, https://doi.org/10.1039/c3ta13049e.

105. P. Karthika, N. Rajalakshmi, and K. S. Dhathathreyan, "Phosphorus-Doped Exfoliated Graphene for Supercapacitor Electrodes," *Journal of Nanoscience and Nanotechnology* 13 (2013): 1746–1751, https://doi.org/10.1166/jnn.2013.7112.

106. Z. S. Wu, A. Winter, L. Chen, et al., "Three-Dimensional Nitrogen and Boron Co-Doped Graphene for High-Performance All-Solid-State Supercapacitors," *Advanced Materials* 24 (2012): 5130–5135, https://doi.org/10.1002/adma.201201948.

107. H. Wang, T. Maiyalagan, and X. Wang, "Review on Recent Progress in Nitrogen-Doped Graphene: Synthesis, Characterization, and Its Potential Applications," *ACS Catalysis* 2 (2012): 781–794, https://doi.org/10.1021/cs200652y.

108. D.-Y. Zhao, H.-L. Wang, H.-P. Qi, and W.-F. Jiang, "N-Doped Graphene Aerogels as Efficient Heterogeneous Catalytic Activators for Peroxymonosulfate to Remove 2-sec-butyl-4,6-dinitrphenol (DNBP) in Aqueous Solution," *Materials Research Express* 7 (2020): 015511, https://doi.org/10.1088/2053-1591/ab664f.

109. X. Yu, Y. Kang, and H. S. Park, "Sulfur and Phosphorus Co-Doping of Hierarchically Porous Graphene Aerogels for Enhancing Supercapacitor Performance," *Carbon* 101 (2016): 49–56, https://doi.org/10.1016/j.carbon.2016.01.073.

110. J. Du, L. Liu, Y. Yu, L. Zhang, Y. Zhang, and A. Chen, "Synthesis of Nitrogen Doped Graphene Aerogels Using Solid Supported Strategy for Supercapacitor," *Materials Chemistry and Physics* 223 (2019): 145–151, https://doi.org/10.1016/j.matchemphys.2018.10.062.

111. Z. Wu, X. Yao, and Y. Xing, "A Review of Nitrogen-Doped Graphene Aerogel in Electromagnetic Wave Absorption," *Micromachines* 14 (2023): 1762, https://doi.org/10.3390/mi14091762.

112. R. Shu, G. Zhang, C. Zhang, Y. Wu, and J. Zhang, "Nitrogen-Doping-Regulated Electromagnetic Wave Absorption Properties of Ultralight Three-Dimensional Porous Reduced Graphene Oxide Aerogels," *Advanced Electronic Materials* 7 (2021): 2001001, https://doi.org/10.1002/aelm.202001001.

113. J. Tang, N. Liang, L. Wang, et al., "Three-Dimensional Nitrogen-Doped Reduced Graphene Oxide Aerogel Decorated With Ni Nanoparticles With Tunable and Unique Microwave Absorption," *Carbon* 152 (2019): 575–586, https://doi.org/10.1016/j.carbon.2019.06.049.

114. A. I. Pruna, A. C. Cárcel, A. Benedito, and E. Giménez, "The Effect of Solvothermal Conditions on the Properties of Three-Dimensional N-Doped Graphene Aerogels," *Nanomaterials* 9 (2019): 350, https://doi.org/10.3390/nano9030350.

115. Z. X. Cai, X. H. Song, Y. Y. Chen, Y. R. Wang, and X. Chen, "3D Nitrogen-Doped Graphene Aerogel: A Low-Cost, Facile Prepared Direct Electrode for H_2O_2 Sensing," *Sensors and Actuators, B: Chemical* 222 (2016): 567–573, https://doi.org/10.1016/j.snb.2015.08.094.

116. Z. Chen, S. Zhao, H. Zhao, Y. Zou, C. Yu, and W. Zhong, "Nitrogen-Doped Interpenetrating Porous Carbon/Graphene Networks for Supercapacitor Applications," *Chemical Engineering Journal* 409 (2021): 127891, https://doi.org/10.1016/j.cej.2020.127891.

117. J. Chen, C. Lin, M. Zhang, T. Jin, and Y. Qian, "Constructing Nitrogen, Selenium Co-Doped Graphene Aerogel Electrode Materials for Synergistically Enhanced Capacitive Performance," *ChemElectroChem* 7 (2020): 3311–3318, https://doi.org/10.1002/celc.202000635.

118. L. Zhang, H. Chen, X. Lu, et al., "Fabrication of N, S Co-Doped Graphene Aerogel for High-Performance Supercapacitors: π-conjugated Planar Molecules as Efficient Dopants and Pillared Agents," *Applied Surface Science* 529 (2020): 147022, https://doi.org/10.1016/j.apsusc.2020.147022.

119. Y. Yuan, H. Lv, Q. Xu, H. Liu, and Y. Wang, "A Few-Layered MoS2 Nanosheets/Nitrogen-Doped Graphene 3D Aerogel as a High Performance and Long-Term Stability Supercapacitor Electrode," *Nanoscale* 11 (2019): 4318–4327, https://doi.org/10.1039/C8NR05620J.

120. L. E, W. Li, J. Sun, Z. Wu, and S. Liu, "N-Doped Carbon Aerogels Obtained From APMP Fiber Aerogels Saturated With Rhodamine Dye and Their Application as Supercapacitor Electrodes," *Applied Sciences* 9 (2019): 618, https://doi.org/10.3390/app9040618.

121. M. B. Arvas, M. Gencten, and Y. Sahin, "One-Step Synthesized N-Doped Graphene-Based Electrode Materials for Supercapacitor Applications," *Ionics* 27 (2021): 2241–2256, https://doi.org/10.1007/s11581-021-03986-2.

122. F. Farbod, M. Mazloum-Ardakani, H. R. Naderi, and H. Mohammadian-Sarcheshmeh, "Synthesis of a Porous Interconnected Nitrogen-Doped Graphene Aerogel Matrix Incorporated With Ytterbium Oxide Nanoparticles and Its Application in Superior Symmetric Supercapacitors," *Electrochimica Acta* 306 (2019): 480–488, https://doi.org/10.1016/j.electacta.2019.03.131.

123. S. Kumari, E. Verma, R. Kumar, et al., "Micropores Within N,S Co-Doped Mesoporous 3D Graphene-Aerogel Enhance the Supercapacitive Performance," *New Journal of Chemistry* 45 (2021): 7523–7532, https://doi.org/10.1039/D1NJ00459J.

124. M. Nazari, M. S. Rahmanifar, A. Noori, W. Li, C. Zhang, and M. F. Mousavi, "The Ordered Mesoporous Carbon Nitride-Graphene Aerogel Nanocomposite for High-Performance Supercapacitors," *Journal of Power Sources* 494 (2021): 229741, https://doi.org/10.1016/j.jpowsour.2021.229741.

125. L. Yang, K. Zhuo, X. Xu, et al., "Anthraquinone-Modified Nitrogen-Doped Graphene Aerogel for Boosting Energy Density of Supercapacitors by Self-Matching of Capacity," *Electrochimica Acta* 393 (2021): 139057, https://doi.org/10.1016/j.electacta.2021.139057.

126. Q. Liu, L. Zhang, H. Chen, et al., "Sulfur and Nitrogen Co-Doped Three-Dimensional Graphene Aerogels for High-Performance Supercapacitors: A Head to Head Vertical Bicyclic Molecule Both as Pillaring Agent and Dopant," *Applied Surface Science* 565 (2021): 150453, https://doi.org/10.1016/j.apsusc.2021.150453.

127. R. Lei, W. Liu, X. Li, et al., "Fabrication of Nitrogen-Doped Graphene/MnO_2 Nanocomposite on 316l Stainless Steel as Binder-Free Electrode Materials for High Performance Supercapacitors," (2025), https://doi.org/10.2139/ssrn.5195953.

128. P. Xu, Q. Gao, L. Ma, et al., "A High Surface Area N-Doped Holey Graphene Aerogel With Low Charge Transfer Resistance as High Performance Electrode of Non-Flammable Thermostable Supercapacitors," *Carbon* 149 (2019): 452–461, https://doi.org/10.1016/j.carbon.2019.04.070.

129. L. Yang, T. Wang, and D. Wu, "Porous Nitrogen-Doped Reduced Graphene Oxide Gels as Efficient Supercapacitor Electrodes and Oxygen Reduction Reaction Electrocatalysts," *Chinese Journal of Chemistry* 38 (2020): 1123–1131, https://doi.org/10.1002/cjoc.201900482.

130. X. Zou, D. Wu, Y. Mu, et al., "Boron and Nitrogen Co-Doped Holey Graphene Aerogels With Rich B–N Motifs for Flexible Supercapacitors," *Carbon* 159 (2020): 94–101, https://doi.org/10.1016/j.carbon.2019.12.018.

131. S. A. Alomari, D. P. Dubal, J. MacLeod, S. Jadhav, C. Padwal, and N. Motta, "Nitrogen, Phosphorus Co-Doped Holey rGO as a Cathode Material for Li-Ion Capacitors (LICs)," *Applied Surface Science* 641 (2023): 158452, https://doi.org/10.1016/j.apsusc.2023.158452.

132. Z. Lu, X. Xu, Y. Chen, X. Wang, L. Sun, and K. Zhuo, "Nitrogen and Sulfur Co-Doped Graphene Aerogel With Hierarchically Porous Structure for High-Performance Supercapacitors," *Green Energy & Environment* 5 (2020): 69–75, https://doi.org/10.1016/j.gee.2019.06.001.

133. A. Ghazitabar, M. Naderi, D. Fatmehsari Haghshenas, and M. Rezaei, "Synthesis of N-Doped Graphene Aerogel/Co_3O_4/ZnO Ternary Nanocomposite via Mild Reduction Method With an Emphasis on Its Electrochemical Characteristics," *Journal of Alloys and Compounds* 794 (2019): 625–633, https://doi.org/10.1016/j.jallcom.2019.04.188.

134. Y. Chen, H. Hao, X. Lu, et al., "Porous 3D Graphene Aerogel Co-Doped With Nitrogen and Sulfur for High-Performance Supercapacitors," *Nanotechnology* 32 (2021): 195405, https://doi.org/10.1088/1361-6528/abdf8d.

135. F. Yang, D. Hegh, D. Song, et al., "Synthesis of Nitrogen-Sulfur Co-Doped $Ti_3C_2T_x$ MXene With Enhanced Electrochemical Properties," *Materials Reports: Energy* 2 (2022): 100079, https://doi.org/10.1016/j.matre.2022.100079.

136. S. Ghosh, S. Barg, S. M. Jeong, and K. Ostrikov, "Heteroatom-Doped and Oxygen-Functionalized Nanocarbons for High-Performance Supercapacitors," *Advanced Energy Materials* 10 (2020): 2001239, https://doi.org/10.1002/aenm.202001239.

137. J. Li, X. Li, D. Xiong, L. Wang, and D. Li, "Enhanced Capacitance of Boron-Doped Graphene Aerogels for Aqueous Symmetric Supercapacitors," *Applied Surface Science* 475 (2019): 285–293, https://doi.org/10.1016/j.apsusc.2018.12.152.

138. T. Jin, J. Chen, C. Wang, Y. Qian, and L. Lu, "Facile Synthesis of Fluorine-Doped Graphene Aerogel With Rich Semi-Ionic C–F Bonds for High-Performance Supercapacitor Application," *Journal of Materials Science* 55 (2020): 12103–12113, https://doi.org/10.1007/s10853-020-04821-1.

139. M. K. Ubhi, M. Kaur, J. K. Grewal, and V. K. Sharma, "Phosphorous- and Boron-Doped Graphene-Based Nanomaterials for Energy-Related Applications," *Materials* 16 (2023): 1155, https://doi.org/10.3390/ma16031155.

140. M. Muhiuddin, A. Z. Khan, N. A. Devi, et al., "Cost Effective Synthesis of Sulfur and Nitrogen Co-Doped Graphene Aerogel and Application in Binder Free Supercapacitor," *Journal of Applied Physics* 136 (2024): 34901, https://doi.org/10.1063/5.0202270.

141. X.-Y. Zhang, S.-H. Sun, X.-J. Sun, et al., "Plasma-Induced, Nitrogen-Doped Graphene-Based Aerogels for High-Performance Supercapacitors," *Light: Science & Applications* 5 (2016): e16130, https://doi.org/10.1038/lsa.2016.130.

142. E. B. Yutomo, F. A. Noor, and T. Winata, "Effect of the Number of Nitrogen Dopants on the Electronic and Magnetic Properties of Graphitic and Pyridinic N-Doped Graphene – a Density-Functional Study," *RSC Advances* 11 (2021): 18371–18380, https://doi.org/10.1039/D1RA01095F.

143. X. Wang, L. Zuo, Y. Wang, et al., "Electrochemical Performance of Nitrogen Self-Doping Carbon Materials Prepared by Pyrolysis and Activation of Defatted Microalgae," *Molecules* 28 (2023): 7280, https://doi.org/10.3390/molecules28217280.

144. S. N. Faisal, E. Haque, N. Noorbehesht, et al., "Pyridinic and Graphitic Nitrogen-Rich Graphene for High-Performance Supercapacitors and Metal-Free Bifunctional Electrocatalysts for ORR and OER," *RSC Advances* 7 (2017): 17950–17958, https://doi.org/10.1039/C7RA01355H.

145. J. Gu, H. Wang, S. Li, et al., "Tuning Pyridinic-N and Graphitic-N Doping With 4,4′-bipyridine in Honeycomb-Like Porous Carbon and Distinct Electrochemical Roles in Aqueous and Ionic Liquid Gel Electrolytes for Symmetric Supercapacitors," *Journal of Colloid and Interface Science* 635 (2023): 254–264, https://doi.org/10.1016/j.jcis.2022.12.127.

146. C. Zhan, Y. Zhang, P. T. Cummings, and D. Jiang, "Enhancing Graphene Capacitance by Nitrogen: Effects of Doping Configuration and Concentration," *Physical Chemistry Chemical Physics* 18 (2016): 4668–4674, https://doi.org/10.1039/C5CP06952A.

147. T. Huang, Y. Long, Z. Dong, et al., "Ultralight, Elastic, Hybrid Aerogel for Flexible/Wearable Piezoresistive Sensor and Solid–Solid/Gas–Solid Coupled Triboelectric Nanogenerator," *Advanced Science* 9 (2022): 2204519, https://doi.org/10.1002/advs.202204519.

148. Z. Deng, C. Gao, S. Feng, et al., "Highly Compressible, Light-Weight and Robust Nitrogen-Doped Graphene Composite Aerogel for Sensitive Pressure Sensors," *Chemical Engineering Journal* 471 (2023): 144790, https://doi.org/10.1016/j.cej.2023.144790.

149. X. Huang, X. Luo, M. Yan, et al., "Better Biocompatibility of Nitrogen-Doped Graphene Compared With Graphene Oxide by Reducing Cell Autophagic Flux Blockage and Cell Apoptosis," *Journal of Biomedical Materials Research. Part A* 112 (2024): 121–138, https://doi.org/10.1002/jbm.a.37624.

150. H. Jin, N. Lai, C. Jiang, et al., "Potential Health Risks of Exposure to Graphene and Its Derivatives: A Review," *Processes* 13 (2025): 209, https://doi.org/10.3390/pr13010209.

151. Y. Wang, K. Xue, C. Yan, et al., "Tuning of Ionic Liquid–Solvent Electrolytes for High-Voltage Electrochemical Double Layer Capacitors: A Review," *Batteries* 10 (2024): 54, https://doi.org/10.3390/batteries10020054.

152. X.-L. Su, M.-Y. Cheng, L. Fu, et al., "Facile Synthesis of 3D Nitrogen-Doped Graphene Aerogel Nanomeshes With Hierarchical Porous Structures for Applications in High-Performance Supercapacitors," *New Journal of Chemistry* 41 (2017): 5291–5296, https://doi.org/10.1039/C7NJ00440K.

153. Y. Chen, L. Sun, Z. Lu, Z. Liu, Y. Jiang, and K. Zhuo, "Preparation of Nitrogen and Sulfur Co-Doped Graphene Aerogel With Hierarchical Porous Structure Using Ionic Liquid Precursor for High-Performance Supercapacitor," *Ionics* 25 (2019): 2781–2789, https://doi.org/10.1007/s11581-018-2785-y.

154. S. S. Shams, R. Zhang, and J. Zhu, "Graphene Synthesis: A Review," *Materials Science-Poland* 33 (2015): 566–578, https://doi.org/10.1515/msp-2015-0079.

155. A. Ambrosi, C. K. Chua, A. Bonanni, and M. Pumera, "Electrochemistry of Graphene and Related Materials," *Chemical Reviews* 114 (2014): 7150–7188, https://doi.org/10.1021/cr500023c.

156. R. S. Edwards and K. S. Coleman, "Graphene Synthesis: Relationship to Applications," *Nanoscale* 5 (2013): 38–51, https://doi.org/10.1039/c2nr32629a.

157. X. J. Lee, B. Y. Z. Hiew, K. C. Lai, et al., "Review on Graphene and Its Derivatives: Synthesis Methods and Potential Industrial Implementation," *Journal of the Taiwan Institute of Chemical Engineers* 98 (2019): 163–180, https://doi.org/10.1016/j.jtice.2018.10.028.

158. H. Bi, K. Yin, X. Xie, et al., "Low Temperature Casting of Graphene With High Compressive Strength," *Advanced Materials (Deerfield Beach, Fla.)* 24 (2012): 5124–5129, https://doi.org/10.1002/adma.201201519.

159. Y. Xu, K. Sheng, C. Li, and G. Shi, "Self-Assembled Graphene Hydrogel via a One-Step Hydrothermal Process," *ACS Nano* 4 (2010): 4324–4330, https://doi.org/10.1021/nn101187z.

160. Y. Chen, Y. Jiang, Z. Liu, L. Yang, Q. Du, and K. Zhuo, "Hierarchical Porous N-Doped Graphene Aerogel With Good Wettability for High-Performance Ionic Liquid-Based Supercapacitors," *Electrochimica Acta* 366 (2021): 137414, https://doi.org/10.1016/j.electacta.2020.137414.

161. S. Feng, L. Yu, M. Yan, J. Ye, J. Huang, and X. Yang, "Holey Nitrogen-Doped Graphene Aerogel for Simultaneously Electrochemical Determination of Ascorbic Acid, Dopamine and Uric Acid," *Talanta* 224 (2021): 121851, https://doi.org/10.1016/j.talanta.2020.121851.

162. QinQin, M. Li, P. Lan, Y. Liao, S. Sun, and H. Liu, "Novel $CaCO_3$/Chitin Aerogel: Synthesis and Adsorption Performance Toward Congo Red in Aqueous Solutions," *International Journal of Biological Macromolecules* 181 (2021): 786–792, https://doi.org/10.1016/j.ijbiomac.2021.03.116.

163. H. Yang, H. Wang, W. Li, et al., "A Simple and Effective Host for Sodium Metal Anode: A 3D-Printed High Pyrrolic-N Doped Graphene Microlattice Aerogel," *Journal of Materials Chemistry A* 10 (2022): 16842–16852, https://doi.org/10.1039/D2TA03294E.

164. S. Ullah, M. Hasan, H. Q. Ta, et al., "Synthesis of Doped Porous 3D Graphene Structures by Chemical Vapor Deposition and Its Applications," *Advanced Functional Materials* 29 (2019): 1904457, https://doi.org/10.1002/adfm.201904457.

165. R. Zan and A. Altuntepe, "Nitrogen Doping of Graphene by CVD," *Journal of Molecular Structure* 1199 (2020): 127026, https://doi.org/10.1016/j.molstruc.2019.127026.

166. R. Han, Y. Cao, P. Li, J. Xie, and X. Chen, "Metal-Plasma Treated Aerogel Materials With Nano-Particle Decoration for Surface Functionalization via Electrical Explosion Method," *Energy Reports* 9 (2023): 213–220, https://doi.org/10.1016/j.egyr.2023.04.061.

167. M. B. Wakchaure and P. L. Menezes, "Graphene Oxide Aerogels: From Synthesis Pathways to Mechanical Performance and Applications," *Processes* 13 (2025): 2375, https://doi.org/10.3390/pr13082375.

168. B. Quan, S.-H. Yu, D. Y. Chung, et al., "Single Source Precursor-Based Solvothermal Synthesis of Heteroatom-Doped Graphene and Its Energy Storage and Conversion Applications," *Scientific Reports* 4 (2014): 5639, https://doi.org/10.1038/srep05639.

169. H. Li, Y. Han, P. Qiu, and Y. Qian, "Plasma-Assisted Preparation of Reduced Graphene Oxide and Its Applications in Energy Storage," *Nanomaterials* 14 (2024): 1922, https://doi.org/10.3390/nano14231922.